PLASMONIC FLUORESCENCE ENHANCEMENT OF POLY(3-HEXYLTHIOPHENE) FOR ORGANIC SOLAR CELL APPLICATIONS

A thesis presented to the faculty of the Graduate School of
Western Carolina University in partial fulfillment of the
requirements for the degree of Master of Science in Chemistry.

By

Jacklyn Claraine Bush

Director: Dr. David D. Evanoff, Jr.
Assistant Professor of Chemistry
Department of Chemistry & Physics

Committee Members: Dr. Carmen L. Huffman, Chemistry
Dr. Channa R. De Silva, Chemistry

March 2012

ACKNOWLEDGEMENTS

First and foremost, I would like to extend my most sincere gratitude towards my research advisor, Dr. Dave Evanoff, for his remarkable leadership, patience, and encouragement throughout this process. The mentoring he has provided throughout this experience will continue to influence me and is greatly appreciated, as is the advice and contributions from my committee members, Dr. Carmen Huffman and Dr. Channa De Silva. Thank you for your time involved in making this possible. I also thank the other faculty members of the department for the outstanding contributions they have made to my education as well as the personal impact they have each had on my life.

I want to thank the WCU Department of Chemistry & Physics and the Faculty Research and Creative Activities Grant for helping to fund this research, as well as LORD Corporation of Cary, North Carolina for the generous donation of a glovebox. I also wish to thank the Clemson University Electron Microscope Facility and COMSET for access to instrumentation.

I wish to offer warm regards and special thanks to my family for their unending support and guidance throughout the years; I attribute my past, current, and future success to them. My mother and father have instilled in me not only the value of hard work but of perseverance. My brother has been an inspiration and a true example of how great sacrifices can lead to greater achievements and the fulfillment of ambitions. To Mom, Dad, and John - thank you.

To Jenna, Nick, Ashley, Brittany, and my fellow students – our friendship has kept me grounded. I am truly happier, wiser, and blessed for knowing each of you.

Lastly, I would like to dedicate this work to the memory of Collin A. Jones and Chief Eric S. Childers; they will always be greatly missed.

TABLE OF CONTENTS

LIST OF TABLES

Table Page

LIST OF FIGURES

Figure Page

LIST OF ABBREVIATIONS

BHJ - Bulk Heterojunction
CNT - Carbon Nanotube
D/A - Donor/Acceptor
EET - Excitation Energy Transfer
EF - Enhancement Factor
HOMO - Highest Occupied Molecular Orbital
ICP-OES – Inductively Coupled Plasma Optical Emission Spectrometry
ITO - Indium Tin Oxide
LUMO - Lowest Unoccupied Molecular Orbital
OD – Optical Density; the unit of extinction
OPV - Organic Photovoltaic
P3HT - Poly(3-hexylthiophene)
PCBM - Phenyl-C_{61}-butyric acid methyl ester
PCE - Power Conversion Efficiency
PCPDTBT - Poly[2,6-(4,4-bis-(2-ethylhexyl)-4*H*-cyclopental[2,1-b;3,4-b]-dithiophene)-*alt*-4,7-(2,1,3-benzothiadiazole)]
PEDOT:PSS - Poly(ethylenedioxythiophene):poly(styrenesulfonate)
PV - Photovoltaic
PVD - Photovoltaic Device
PVP - Poly(vinylpyridine)
SEF - Surface-Enhanced Fluorescence
SERS - Surface-Enhanced Raman Spectroscopy
SPR - Surface Plasmon Resonance
TEM – Transmission Electron Microscopy
UV-Vis - Ultraviolet Visible Extinction Spectroscopy
V_{OC} - Open Circuit Voltage

ABSTRACT

PLASMONIC FLUORESCENCE ENHANCEMENT OF POLY(3-HEXYLTHIOPHENE) FOR ORGANIC SOLAR CELL APPLICATIONS

Jacklyn Claraine Bush, M.S.

Western Carolina University (March 2012)

Director: Dr. David D. Evanoff, Jr.

Solar cells are becoming an attractive alternative energy source considering the need to lessen dependence on nonrenewable energy sources such as fossil fuels. Organic photovoltaics (PVs) are inexpensive to produce, flexible, and eliminate many potential environmental hazards. However, organic solar cells are greatly limited in their capacity to efficiently convert sunlight into usable energy.

Herein, an approach to increase the efficiency of exciton formation of poly(3-hexylthiophene) (P3HT), a common polymer used in organic solar cell devices, is described. This enhancement occurred by adding silver nanoparticles to the polymer surface. The metal nanoparticles cause an increased exciton excitation rate within the polymer through a mechanism known as surface-enhanced fluorescence (SEF). Specifically, P3HT fluorescence is increased when molecules are within the near fields of a metallic nanoparticle under plasmon resonance conditions. Theoretically, the enhancement of polymer exciton formation should correlate to heightened efficiency when utilized within a PV device.

Silver nanoparticles are an attractive choice for SEF, as these particles possess strongly scattering local fields, a highly-polarizing, non-radiative field that extends deep into the particles' environment, and a plasmon resonance that overlaps well with both the

absorption of P3HT and the solar spectrum maximum. In this study, silver nanoparticles with diameters of 15-153 nm have been synthesized in order to optimize the fluorescence enhancement factor of P3HT films of comparable thickness to those used in organic solar cells.

Another aspect of this work was the development of a basic and reliable methodology for the preparation and analysis of P3HT/silver films. This standard protocol allows for the future application of our findings into actual devices and is vital considering the lack of current literature reporting studies of fluorescence effects produced from particles in this size range.

It was determined that the addition of silver nanoparticles to the P3HT surface produced a significant increase in fluorescence. Also observed were higher enhancement factors associated with increasing nanoparticle diameter due to the scattering properties associated with larger particles. The enhancement associated with increasing particle size occurred independently of spin-coating speed of the polymer or silver nanoparticle concentration, though additional studies in the future are required for better methods of P3HT film deposition and the accurate measurement of particles underneath the polymer layer. Once enhancement parameters are optimized, studies will also include the incorporation of these particles into a device.

CHAPTER ONE: BACKGROUND

1.1 Introduction to Organic Solar Cells

With the cost of traditional energy continuously on the rise, there is an increasing need to develop newer, more cost-effective and efficient means of energy production. Ideally, an innovative new energy source would produce cleaner energy with a lower manufacturing cost, while simultaneously remaining competitively efficient. The operation of a photovoltaic device (PVD) can be attributed the photoelectric effect, in that free electrons are generated by exposure to electromagnetic radiation. Solar cells, an example of photovoltaic devices powered by the solar emission spectrum, are increasing in popularity due to their potential to lessen dependence on nonrenewable energy supplies such as fossil fuels. Usually comprised of silicon, solar cells are relatively expensive to produce, which has spurred interest in less expensive photovoltaic devices, such as dye-sensitized cells and other organic-based structures. Organic solar cells are PVDs that allow energy production by using organic materials in the place of the more expensive inorganic material. These organic photovoltaic (OPV) devices possess the potential to decrease dependence on traditional energy sources while offering a significantly lower manufacturing cost, flexibility, and the added benefit of low device mass.[1]

1.2 Poly(3-hexylthiophene)

Poly-3-hexylthiophene (P3HT) is the semiconducting polymer typically utilized in organic photovoltaic devices due to its attractive properties. A monomer unit of the polymer is displayed in **Figure 1a**.

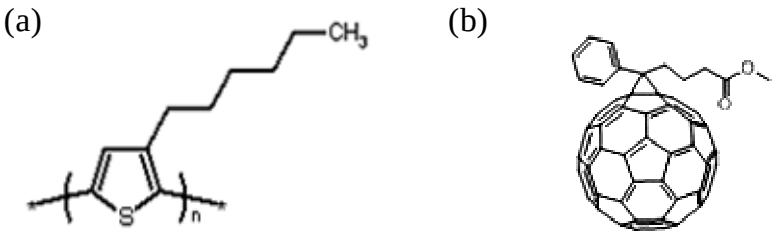

Figure 1: Typical hole and electron transport materials in OPVs. A monomer unit of (**a**) poly(3-hexylthiophene) and (**b**) the structure of phenyl-C_{61}-butyric acid methyl ester.

The energy gap separating the highest-occupied molecular orbital (HOMO) and the lowest-unoccupied molecular orbital (LUMO) energy levels of this polymer is particularly well-matched to the frequency of maximum solar emission. As shown in **Figure 2**, the absorption spectrum of poly-3-hexylthiophene nearly completely overlaps the spectrum of solar irradiation. The primary drawback of P3HT, and of organic solar devices in general, is the polymer's inability to *efficiently* convert photons into usable work, mainly due to short exciton lifetimes, as will be described below.

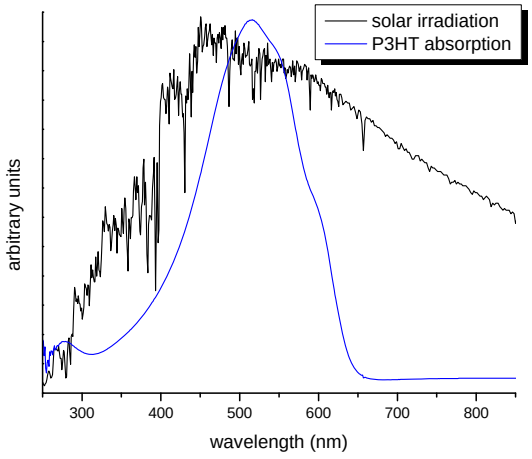

Figure 2: Spectra of P3HT absorption (blue) and solar irradiation (black).[2]

1.3 Solar Cell Structure and Function

The typical structural design of an organic solar cell involves an aluminum cathode and gold- or indium tin oxide-coated anode separated by layers of various materials. Photons are absorbed by the P3HT layer and elevate valence electrons into the conduction band, thus generating electron-hole pairs, i.e. excitons. Due to a small potential applied across the film during device operation, these excitons dissociate, and the electrons and their corresponding holes travel in opposing directions towards the electrodes. During migration, electrons and holes may recombine, producing fluorescence, or may be separated enough to contribute to a photocurrent within the device. A layer of poly(3, 4-ethylenedioxythiophene)-poly(styrenesulfonate) (PEDOT:PSS) prevents the accumulation of holes at the P3HT-anode interface by decreasing the work-function mismatch. A monomer unit of PEDOT:PSS is shown in **Figure 3**.

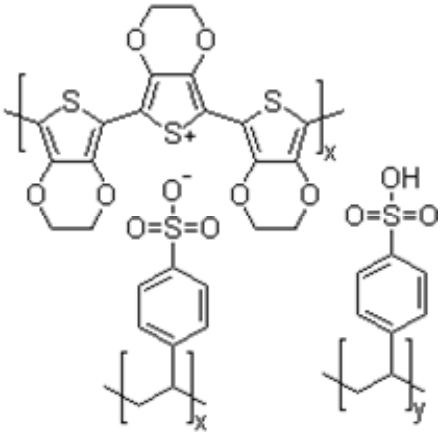

Figure 3: Structure of poly(3,4-ethylenedioxythiophene):poly(styrenesulfonate).

An electron-accepting material, typically either the fullerene derivative phenyl-C_{61}-butyric acid methyl ester (PCBM), cf. **Figure 1b**, or nano-sized anatase titania, is dispersed within the P3HT matrix, creating a bulk heterojunction (BHJ) device. Having multiple p-n junctions in the film help segregate the electrons, preventing them from recombining with the holes that are formed in the P3HT and promoting electron advancement towards the cathode. Once these electrons reach the aluminum cathode, the electrons pass through an external circuit to power a load. Due to limited exciton lifetime or lack of mobility, organic solar cells do not typically generate a significant amount of current. On average, organic solar cells possess an efficiency of approximately 5%,[3-5] which implies that around 5 out of every 100 photons are converted into usable work energy. This low efficiency can be attributed primarily to the short exciton diffusion lengths within the organic solar cell device.[6] Work has been done to optimize the P3HT thickness in a device.[1] Thinner films allow electrons and holes to reach the electrodes without recombination, but thicker films increase the concentration of photogenerated excitons.

1.4 Development of Organic Photovoltaics

Polymer-based solar cells are a relatively new technology within the broad field of photovoltaics (PVs). However, the concept of utilizing light to produce usable energy via inorganic materials has existed for generations. The conceptual basis for all PVDs originates back to the initial understanding of the photoelectric effect, the ejection of electrons from a material when exposed to electromagnetic radiation, which has been accredited to Henri Bacquerel in the 1800's as he observed a photocurrent by placing silver bromide or silver chloride covered platinum electrodes into an aqueous solution.[7]

The true debut of the field of PVs began in the early 19th century through the observation of photoconductivity in solid anthracene by Pochettino and Volmer.[7] Further examination of photovoltaics was later performed in the 1950's, incorporating studies of chlorophyll and other organic compounds. It was also discovered during this time that organic compounds could be used as photoreceptors for imaging systems.[7, 8] Increased studies of the conductive properties of organic materials, such as dyes like methylene blue,[9] led to greater commercial interest as well. Thirty years later marked the first application of organic polymers in photovoltaic cells, though yielding low efficiencies of well below 0.1%.[7] In 1986, a polymer-based cell was designed with a power conversion efficiency (PCE) of 1.0%, devised by Tang via the combination of an acceptor and donor, or p-n junction, within the cell.[7, 10] This concept of a single donor and acceptor layer is commonly referred to as a bilayer OPV. Increase in the efficiency has been limited in this type of system due to the distance electrons and holes must travel for dissociation in this system.[11] As a result, the bulk heterojunction (BHJ) concept has been utilized in a variety of more current PV donor-acceptor structures. BHJ devices incorporate a network of donor and acceptor materials to ensure that all excitons reach a donor/acceptor interface within their diffusion length;[12] failure to reach a donor/acceptor, or D/A, interface results in exciton recombination. Advances in this area of BHJ devices include dye/dye,[13, 14] dye/polymer,[15] and polymer/polymer blends.[7] Polymer/fullerene blends have also become widely investigated over the course of recent years and have produced the more promising results for the future of OPVs.[7] Recent studies report the production of OPVs with efficiencies as high as 7-8%,[16] up from the typical 5%,[3-5] due primarily to the incorporation of low bandgap donor material and

better control over the morphology of the D/A material network.[16] As semiconducting polymers under an applied field tend to degrade, scientific research has also focused on longer shelf and operational lifetimes. Upgrading manufacturing processes and materials has also been of interest, all with the intention of increasing the demand and availability for OPVs on the market.

Reports in the year 2000 estimated that photovoltaics contributed to 277 MW worldwide, equivalent to a value of US$ 1 billion and exhibited growth over the past decade of 15-25%.[17] Despite advancements and persistent interests in the potential for polymer-based cells, reports from 2010 claim that the market for solar devices has been and remains dominated by inorganic, typically silicon-based, structures.[18] This includes various forms of crystalline silicon, such as single-crystal and cast poly material.[19] Other materials utilized in inorganic photovoltaics include gallium arsenide and sulfide salts.[20] The efficiency of today's inorganic solar devices have reached a capacity for efficiencies as high as approximately 40%, a marked increase from the 6% efficiency of the first silicon-based solar cell produced in 1954 by Bell Laboratories.[7, 21] Still, the potential for significantly lessened material and manufacturing costs drives further studies into developing competitive semiconductor PVDs. For example, the organic molecules or plastics required for these devices may be synthesized in a cheaper and more simplified manner than their inorganic counterparts. In addition, organic solar cells may also be produced in long, flexible rolls by faster processes such as screen printing.[22]

1.5 Device Limitations

Numerous disadvantages still currently exist with polymeric devices that hinder their ability to effectively compete with other modern forms of energy production. For

example, problems that plague this industry include low conversion efficiency due to the poor spectral match between polymer layer absorption (typically below 650 nm) and solar flux, high exciton recombination, as well as instability and degradation with exposure to oxygen and/or high temperatures.[23] Despite drawbacks, the versatility and capacity of organic materials for light harvesting continue to prove their potential as a contributor to alternative energy. OPVs are unable to completely eliminate dependence on more traditional energy sources such as fossil fuels or inorganic solar structures considering the inability to compete with much higher efficiencies. However, polymeric devices do show promise in becoming a popular means of providing particular niche markets the provision of environmentally nontoxic, sustainable energy for specific, short-term applications.

1.6 Current Enhancement Methods

Due to the prospective advantages of OPVs, investigations of methods for their improvement have become a broad subject of study in worldwide research areas. Studies include changing donor/acceptor compositions to enhance charge transfer and transport,[5] producing materials with lower bandgaps to include broader absorption ranges,[16] as well as structure modification to promote lasting stability while consistently maintaining competitive manufacturing and processing prices and avoiding potentially harmful environmental risks.[1] Other experiments have incorporated the adjustment of other parameters such as varying polymer spin coating speed and time,[5] changing the identity of the donor/acceptor materials,[6] solvent type,[5] temperature,[11] adding electric and/or magnetic fields,[5]and adding other compounds such as lithium fluoride to increase open circuit voltage, or V_{OC},[5] the maximum voltage available within a solar cell when zero

current is applied. Lithium fluoride is placed between the anode and active layer and acts as a protective barrier between the metal and organic material,[24] preventing chemical and physical damage as well as oxygen permeation into the polymer.[25] The addition of carbon nanotubes (CNTs) to the polymer/fullerene blend has also been studied and has resulted in a marked increase in conversion efficiency; as high as 40% more than devices devoid of the CNT additives. The CNTs, dispersed throughout the polymer:fullerene BHJ, contribute to enhancement through their high charge carrier mobility and wideband photo-absorption.[26]

As previously mentioned, the study of organic materials possessing low bandgaps within a PVD has been an active area of recent research.[16] The mismatch between absorption in the photoactive layer and the spectrum of the solar flux has long been an issue within OPV devices and has resulted in low utilization of incident light. The goal of decreasing the bandgap would be increasing the ability to effectively capture more sunlight. Ideally, the absorption peak would broaden without shifting the entire spectrum, indicating that more visible light was absorbed. However, this is not typically the case. Decreasing bandgap shifts a spectrum to the red, typically without broadening the peak. P3HT has been reported as the primary donor material chosen within the best performing polymeric devices with the fullerene derivative [6,6]-phenylC_{61}-butyric acid methyl ester (C_{61}-PCBM) as the acceptor.[27] Possessing a bandgap of 1.9 eV, the absorption of P3HT occurs at wavelengths shorter than 650 nm. At at this wavelength, only 22.4% of incident photons are absorbed.[28] Lower bandgaps, ideally around 1.4 eV, increase the likelihood of absorption in the red and infrared regions, however, bandgaps that are too low begin to jeopardize the overall PCE of the cell as a result of a decrease in

the V_{OC}.[28] Efforts reported by Cai, et al. include blending four low bandgap polymers, synthesized by $FeCl_3$ oxidative polymerization, within a device and observing electrochemical and photovoltaic output. Bandgaps ranged from 1.0 – 1.9 eV, suitable for PV devices, yet yielded results of limited success with a conversion efficiency of approximately 1.08%.[29] Studies conducted by Peet, et al. involved replacing the P3HT and C_{61}-PCBM donor and acceptor material, which are reported as being limited to an approximate 5% efficiency, with the low bandgap polymer poly[2,6-(4,4-bis-(2-ethylhexyl)-4*H*-cyclopental[2,1-b;3,4-b]-dithiophene)-*alt*-4,7-(2,1,3-benzothiadiazole)] (PCPDTBT) and a C_{71}-PCBM fullerene, respectively. PCPDTBT was chosen due to its desirably low bandgap of 1.46 eV and therefore its ability to absorb further into the infrared region. The acceptor C_{71}-PCBM was selected due to the greater overlap with the solar spectrum, produced through its reportedly higher absorption in the visible region than C_{61}. This group also experimented with the incorporation of alkanethiol-stabilized gold nanoparticles into the polymer blends, and also report enhanced phase separation by adding small concentrations of alkanethiols to the solutions from which the films are spin cast. An average performance efficiency was established between 5.2-5.8% for 1,000 devices produced.[27] Other groups report efficiencies as high as 6.7% with low bandgap polymers with the development of inverted organic solar cells. Within these inverted devices, a high work-function, air-stable metal such as gold or silver serves as an anode and aides in collecting holes while a bottom cathode of transparent indium tin oxide (ITO) collects electrons. Metal oxides, also air-stable, are dispersed among the active layers and electrodes and contribute to charge extraction.[16] A variety of problems exist with low bandgap polymers and their applications in solar cells, however. For example,

while low bandgap polymers tend to absorb well in the infrared region there are areas within the visible region that are sacrificed as a result. Additionally, these polymers tend to exhibit poor hole mobility as well as low solubility for processing, which hinders their ability to entirely replace the typical donor/acceptor materials of P3HT and C_{61}-PCBM within solar devices.[30]

A lack of stability is also a prevalent problem among OPVs. Typically, exposure to air and water vapor, as well as continuous photon bombardment and etching of ITO from the acidity of P3HT and PEDOT:PSS layer, rapidly degrade organic solar devices during use.[23] A variety of efforts have been taken to decrease the rate at which these devices break down and lose efficiency. General steps taken to prevent these problems include encapsulation from air and water to prevent rapid oxidation of the low work-function cathode and anode, though this also contributes to unwanted increases in manufacturing and production costs.[16] Efforts by Krebs et al. describe the enclosure of the devices in a polyethylene terephthalate lamination for prolonged “round robin” studies between labs and report maintained stability over long periods of time and various modes of transportation.[31] The aforementioned inverted OPV structures also have increased stability due to the modifications to the cell structure and exhibit an ability for maintaining 85% original efficiency for up to 32 days of exposure in air.[16]

Other attempts at enhancement include incorporating metal nanoparticles into the photovoltaic devices. Research conducted by Wu et al. describes applying 45 nm gold nanoparticles to the anodic buffer layer within the structure and observed significant increase in enhancement. PCE was improved to 4.24%, up from a value of 3.57% for structures without the gold particles.[32] Enhancements have also been observed within

OPVs by incorporating 13 nm silver nanoparticles in the device by pulse-current electrodeposition. Enhanced efficiency was observed with an increased PCE from 3.05% without silver to 3.69% with the presence of nanoparticles.[33]

1.7 Metal Nanoparticles and Plasmon Resonance

Applications for metal nanoparticles have existed for centuries, dating back to use in medieval stained glass windows[34] and during the fourth century AD with the bronze-lined Roman Lycurgus Cup.[34, 35] The presence of nanoparticles within the cup produced the transmittance of red light and scattering of green light, respectively.[35] Much later in the 1850's, Faraday, based on his observations of a thin gold leaf's ability to transmit green light, contributed to a greater understanding of interactions between light and metal nanoparticle suspensions and metal thin-films.[35, 36]

Nanoparticles have long been employed in various applications but have become a subject of vast study over recent decades through better understanding of the many optical properties and applicability offered. Metal nanoparticles possess high surface area-to-volume ratios and many interesting physical and chemical properties.[37] The ability to synthesize nanoparticles of various materials, such as silver or gold,[35] by either chemical or physical processeses[38] and of notable stability,[35] as well as the ability to fine tune particles for specific applications, also makes them attractive for many areas of research.

Currently, growing areas of nanoparticle-focused research include the incorporation of metallic nanoparticles into PV or other organic-based structures. Metal nanoparticles have a broad variety of applications, and their use has been studied in other

areas such as catalysis and photonics,[39] diodes,[40] cancer cell imaging,[41] biosensors, and bioarrays.[42]

A very interesting aspect of metal nanoparticles is their ability to exhibit a phenomenon known as plasmon resonance, also termed surface plasmon polariton resonances. Plasmon resonance in nanoparticles of Cu, Ag, and Au occurs in the visible region.[35] The concept of plasmon resonance was described by Mie in 1908 as he applied spherical particle boundary conditions to Maxwell's equation,[43] from which he calculated scattering, absorption, and extinction cross-sections for gold nanoparticles. Based on his calculations, Mie was able to predict dipole electric and magnetic fields and describe various components of the particles' resonance.[35] The contributions of Mie have been a valuable asset in explaining many experimental results since that time.[43]

Plasmon resonance is described as the collective oscillation of the particles' conduction electrons[44, 45] when excited by an electromagnetic wave.[44] Optical polarization is produced as the result of the electronic oscillation and generates strong scattering and absorption when the particle plasmon occurs at a resonant frequency;[45] in other words, the electrons begin to oscillate throughout the crystal lattice in sync with the wavelength of interacting light. This electronic oscillation is due to the conduction electron acceleration by the incident light's electric field, restoring forces that are produced within the particle and surrounding medium, as well as the confinement of the electrons to areas smaller than the wavelength of incident light.[35] Among the optical properties generated by plasmon resonance is the ability for the confinement of surrounding light,[46] or the ability to draw in more light than is physically incident on the particle surface. Excitation of the plasmon resonance also initiates the production of an

electromagnetic field comprised of both radiative and local non-radiative fields. The length to which these fields extend affect the manner in which the particles contribute to surface-enhanced phenomena.[35]

1.8 Surface-Enhanced Fluorescence

Luminescence is the emission of light occurring as a result of electron relaxation from an excited state. More specifically, fluorescence is the emissive relaxation from an excited singlet state.[47] Fluorescence can be quantified as quantum yield, which describes the fraction of excitations that lead to relaxation through emission rather than through non-radiative internal/external conversion processes. Enhancement of a fluorophore can occur by its placement within the near fields of metal nanoparticles[48] and by interactions between excited molecules and the surface of metals.[49] This is known as surface-enhanced fluorescence (SEF), or metal-enhanced fluorescence. The plasmon-induced light confinement exhibited by such particles allows a more concentrated flux of photons onto the fluorophore, thereby increasing light absorption and the generation of more electronic excitation.

1.9 SEF Studies and Applications

The numerous uses for metallic nanoparticles as well as their application to fluorescence enhancement of organic materials such as polymers and dyes have inspired much interest in the research areas of chemistry, physics, and medicine. The first reports on SEF emerged in the 70's and 80's.[48, 50] In the early 1980's, Weitz studied the effects of placing fluorescent molecules on roughened silver-island surfaces and reported fluorescence several orders of magnitude higher than when the fluorophores were placed on substrates of silica.[49] In the mid-90's, Lakowicz also observed surface-enhanced

fluorescence in bovine serum albumin and avidin by applying them to colloidal-coated surfaces and silver-island films, as well as the distance dependence between the metal and the enhanced material. Results showed 50% fluorescence enhancement of the fluorophore with silver colloid-coated substrates. Lakowicz also reported an average fluorescence enhancement of an order of magnitude for fluorophores on silver-island films and an optimal distance between metal surface and fluorophore of approximately 70-100 Å.[48] In 1995, Chumanov et al. reported similar distance-dependence studies by placement of a fluorescein-labeled phospholipid on glass or quartz slides coated with gold or silver colloids with spacer shells present. Increasing the number of spacers separating the fluorophore and metal particles in turn decreased the capacity for surface-enhanced fluorescence and also produced significantly weaker Raman signals.[51] More current studies include the incorporation of metal nanoparticles, based on optical and catalytic properties, into Teflon AF with the purpose of observing surface-enhanced phenomena. Teflon AF is a particular material typically utilized as an optical coating, within liquid-core wave-guides, and as a surface-modifier for increased sensitivity in plasmon resonance measurements.[37] Other work includes studies reported by Zheng et al. that describe the addition of gold nanoparticles capped with 3-mercaptopropionic acid to an aqueous solution of acridine orange, resulting in >80 times enhancement in fluorescence. Benefits associated with this study also include a low toxicity of the particles and applications in areas such as DNA and RNA detection.[52] Gold nanoparticles have also been utilized for the fluorescence enhancement of other dyes such as rhodamine B,[53,54] further developing the potential for the use of such dye-metal complexes in areas such as medical imaging and biotechnology.[54] Other advantageous

qualities of plasmon-induced fluorescence enhancement of organic molecules is decreased degradation rates due to shortened excited-state lifetimes as well as increased efficiency by greatly decreasing a fluorophore's radiative decay rates.[50]

Based on the concept of SEF, metallic nanoparticles can also contribute to increased efficiency within a broad range of devices such as an organic-based PVD, where enhancement occurs by the increase of photon absorption within the film as well as the number of generated excitons.[50, 55] SEF has been also observed in multi-particle systems, as well as single-particle samples[56] and particle island films.[52] SEF holds promise for contributing to areas such as biotechnology and medical diagnostics.[48] Therefore, improving the sensitivity is an important focus.[50]

Despite many advantages, one particular problem recognized with SEF is the particle-induced excitation energy transfer (EET), a non-radiative manner of decay, from the fluorophore to the metal particle. This results in sometimes strong fluorescence quenching which competes against enhancement of efficiency. Efforts to decrease quenching include studies of optimal distance between nanoparticle and fluorophore. Other experiments for maximizing the overall fluorescence enhancement include varying parameters such as distance between metal particles in multi-particle systems, orientation of the fluorophore and the role of solvent,[50] as well as the particular excitation wavelength[52] and local refractive index.[58] Efforts to reduce quenching have been developed by Guererro and Acoca in providing ultrathin silica shell coatings to the metallic nanoparticles, providing isolation from the probed materials.[57,59] It was determined that silica shell layers of less than 5 nm resulted in fluorescence quenching. Layers thicker than this width, however, minimized quenching and also contributed to

SEF.[59] Research conducted by Li et al. further supports that silica- or alumina-coated gold particles promote surface-enhanced Raman spectroscopy (SERS), which originates from interactions between molecular dipole and rough metal surfaces.[49] The gold particle monolayer is described as "smart dust" that allows the nanoparticles to conform to a variety of surface architectures, eliminates particle agglomeration, and as mentioned previously, provides a barrier between particle and probed material. Results obtained with the shell-coated gold particles showed enhanced Raman signals that may be applied to areas such as pollutant, explosive, or drug inspection, as well as food safety.[57]

SEF, SERS, and other uses for nanoparticles are not only limited to spherically shaped particles but are broadened through the incorporation of nanorods,[50] nanowires,[60] nanocubes,[61] and nanoplates.[58] For example, it has been reported that cadmium sulfide silver nanoplates have been used for enhanced cancer cell imaging[58] while the effects of individual silver nanocubes on excimer emission has also been studied via single-particle spectroscopy[62] and also reportedly contribute to the enhanced luminescence of europium complexes.[61] Silver nanowires have also been reported as having high SEF and SERS activity.[60]

1.10 Future Applications

The versatile applications of organic-based PVDs include items such as light-emitting diodes, transistors, and sensors.[63] Future applications also include "smart clothing,"[64] which encompasses the incorporation of organic solar cells onto clothing with the capability of powering .mp3 players or cell phones. Remote regions would also be provided an effective means of powering laptops and radios while reducing environmental impact. The ever-expanding possibilities for OPVs have generated much

interest and investigation into various methods of increasing the overall efficiency of the devices. Pending their enhancement to a comparably competitive power conversion efficiency, these devices will be made more readily available to the public in the near future.

CHAPTER TWO: INTRODUCTION TO RESEARCH

The purpose of this research is to explore means of enhancing the fluorescence of P3HT for future application in OPVs. The focus of this research lies in increasing the number of generated excitons, or electron-hole pairs, within P3HT. We believe increasing the amount of excitons within the polymer layer will, in turn, produce more electrons that can reach the cathode in a photovoltaic device, thus increasing photocurrent output. To clarify, this research has not included the study of enhanced photocurrent output in photovoltaic devices. However, the enhancement of polymer fluorescence as observed in this research should directly correlate to increased device efficiency within an OPV structure.

Another important aspect of this research is to establish the groundwork necessary for future work which includes incorporating our findings into a device. Considering the lack of current literature reporting enhancement produced through particles of the sizes described herein, we have also focused on determining a basic and reliable methodology for experimentation. An understanding of the optimal sample preparation conditions and measurement standards are vital before pursuing enhancement within a photovoltaic device.

Enhancement within a device should occur via the same mechanism as surface-enhanced fluorescence, in that the number of excitons generated during excitation will increase when silver nanoparticles are placed within close proximity of the P3HT polymer. As mentioned previously, the plasmon resonance, or collective oscillation of a silver nanoparticle's conduction electrons, produces many of the unique optical

properties of silver, such as the generation of electromagnetic fields that extend from the surface of the particle. Likewise, the plasmon resonance allows each nanoparticle to extinguish more light than is physically incident on its surface.[35] This provides the particle's ability to direct a more concentrated flux of photons onto the layer of P3HT, thus increasing the density of photons into the polymer and allowing for increased exciton formation which is manifested as enhanced fluorescence.

The goal has been to observe how P3HT fluorescence enhancement is affected by the addition of silver nanoparticles to the polymer surface and determining the conditions that provide the maximum enhancement factor (EF). These parameters include the size of the silver nanoparticle size, concentration of particles applied to the polymer, and the thickness of the P3HT active layer.

Initially, we considered examining absorption enhancement that occurs when silver is applied to P3HT. Silver extinction from larger particles produces a broad spectrum. Based on ultraviolet-visible extinction spectroscopy (UV-vis) experiments conducted during this project, difficulty arises in resolving P3HT absorption enhancement, considering the tendency of the silver extinction spectrum to overlap with polymer absorption. An example extinction spectrum of a P3HT film, a film of 118 nm silver particles prepared from a suspension with an optical density (OD) equal to one, and a film of P3HT with the same silver nanoparticles on glass slides is shown in **Figure 4.**

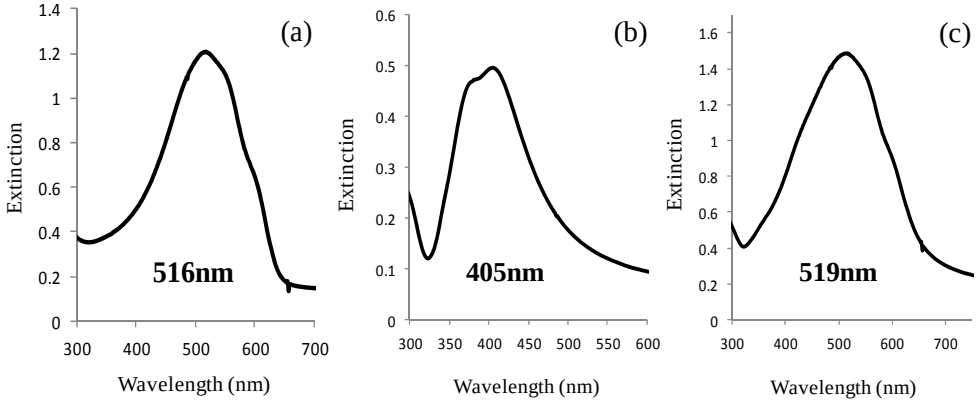

Figure 4: UV-vis spectra of (a) P3HT film absorption, (b) silver particle film extinction, and (c) P3HT film with underlying silver nanoparticles.

The hypothesis was that a noticeable correlation could be observed between maximized P3HT fluorescence and variations in the silver nanoparticle diameter considering how light is extinguished by a particle is a function of size. Extinction refers to the summation of a particle's light absorption and scattering. It has been previously reported that silver particles less than 30 nm in diameter exhibit only absorption and no scattering while for larger particles, for example those with 120 nm diameter, scattering dominates absorption.[65] It was expected that fluorescence enhancement would increase with larger particle diameters before reaching a consistent maximum due to the fact that once the diameter becomes too large the particles would protrude through the polymer layer.

Eight silver particle sizes have been observed during this study and range in diameter from 15 to 153 nm. All silver particle diameters have been verified via scanning and/or transmission electron microscopy (TEM). Images of the particles as well

as their corresponding maximum dipole wavelengths, diameters, and diameter standard deviations are displayed in **Figure 5**.

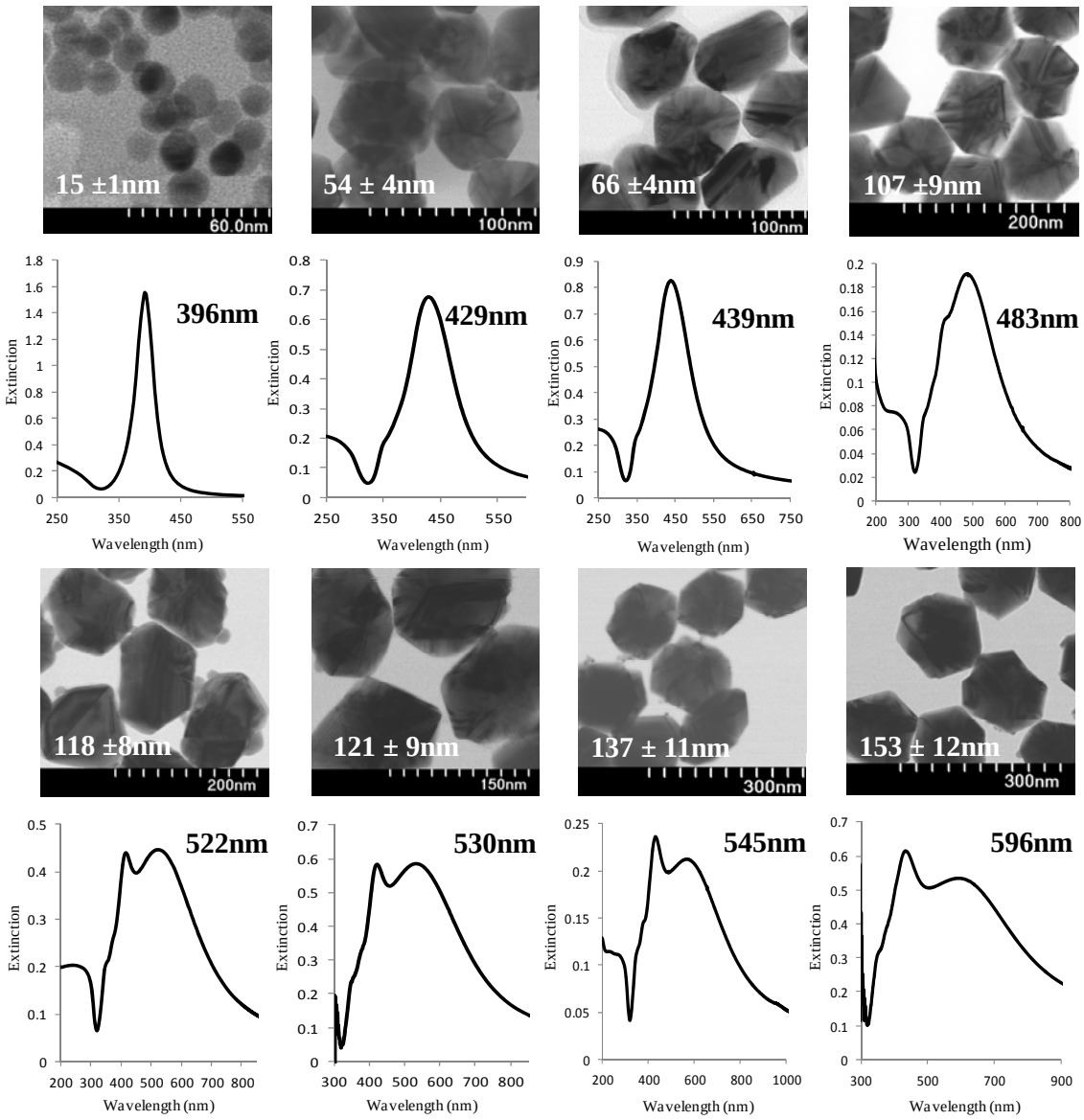

Figure 5: TEM images of the eight silver suspensions studied including mean particle diameters in nanometers and size standard deviations. Also included are corresponding extinction spectra and maximum dipole wavelengths.

Varying the concentration of the silver was also expected to produce a noticeable correlation with polymer fluorescence considering the tendency of silver to couple at higher ODs. In previous studies conducted on the *absorption* enhancement of P3HT, it was determined that there exists an optimum spacing between nanoparticles with diameters of 10 nm.[39] Shen et al. discusses a correlation between increased particle spacing and decreased enhancement. It was observed that structures containing silver nanoparticles spaced far from each other began to resemble those possessing no silver. The group also reports maximum enhancement factor of 1.56 within a 33 nm thick active layer occurring for particles of a mean diameter of 24 nm spaced approximately 40 nm from each other.[39] However, there appears to be a lack of present literature discussing the effects produced from silver particles of larger sizes. Therefore, studying the effect of the concentration of the broad range of larger particles utilized during this research is important, considering the majority of similar efforts reported elsewhere include only the results from significantly smaller particles.[39]

For these experiments, concentrations of the silver suspensions have been divided into ODs of 1, 3, and 5 and applied to glass sample slides. It is important to note that the ODs of the particle films are less than that of the corresponding original suspensions from which they were prepared. We theorized that the higher concentrations would lessen fluorescence enhancement due to the fact that higher concentrations of particles tend to lead to extinction coupling, in which the plasmon resonance occurs within collections of closely spaced particles. **Figure 6** shows UV-Vis extinction spectra from 118 nm silver on glass slides prepared from ODs of 1, 5, and 100 and shows that coupling develops as the concentration increases. The sharp extinction peak produced by the sample prepared

from a suspension of OD 100 is evidence of particle coupling, as opposed to the broad spectrum of an OD 1 sample. As coupling of larger particles increases, plasmon relaxation shifts from mainly scattering to mainly absorption. The apparent loss of radiative relaxation would seemingly serve to decrease SEF.

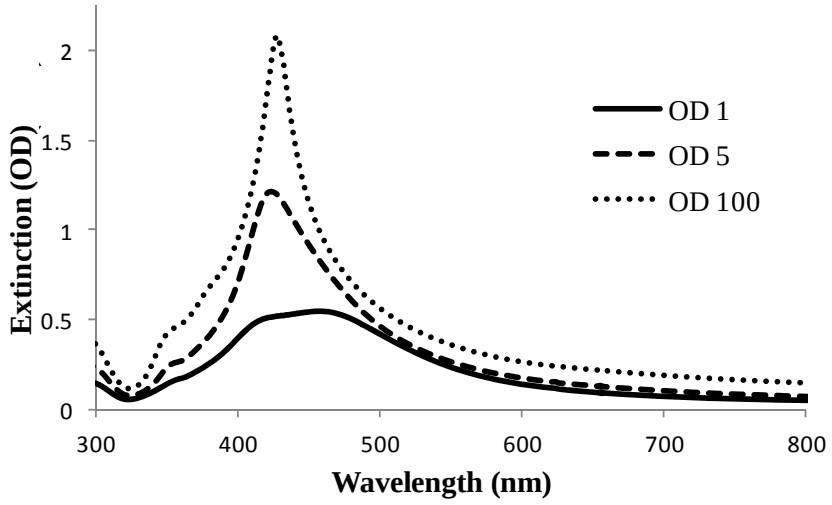

Figure 6: Extinction data collected from 118 nm silver particles adhered to glass slides from ODs 1, 5, and 100 indicative of particle coupling.

The thickness of P3HT applied to the silver nanoparticle layer was also varied to determine the most favorable ratio between fluorescent material and nanoparticles. In addition, the thickness of the active layer dictates the absorption of incident light as well as the likelihood of charge carrier recombination. It has been previously determined that thicker active layers (~196 nm) will exhibit the greatest amount of light harvesting.[39] However, layers of this thickness also suffer the disadvantage of high charge

recombination. Thin layers, approximately 40 nm, maintain less capacity for light absorption though they offer the advantages of higher carrier collection in addition to a lower material cost.[39] For this study, the P3HT active layer has been spin-cast at speeds of 2,500, 3,500, and 4,500 RPM, yielding polymer layers of different thicknesses as determined via contact profilometry. It was predicted that spin-casting at various speeds would yield polymer films of corresponding thicknesses, for example, higher speeds would produce thin films while slower speeds would result in a thicker layer.

The goal of this project has been to determine conditions for the maximum fluorescence enhancement of P3HT by generating more excitons within the polymer. The primary focus was determining the particular combination of P3HT layer thickness with silver particle size and concentration to provide the greatest EF. In addition to observing the particular influence of each variable on P3HT fluorescence enhancement, optimal sample preparation and measurement parameters were also investigated, establishing the foundation for future experimentation with devices.

CHAPTER THREE: EXPERIMENTAL

3.1 Materials

Silver oxide (99+%) was acquired from Alfa Aeser. Water with a resistivity of 18.2MΩ was obtained from a Barnstead NANOpure Diamond system with a 0.2μm hollow fiber filter. Hydrogen gas (research grade, 99.9999%) was received from National Specialty Gases. A 50,000 MW poly(3-hexylthiophene) (99+%), regioregular, electronic grade, was purchased from Rieke Metals Inc. and was stored and protected from sunlight inside the glovebox. Chloroform (99.9%), reagent grade, was acquired from Pharmco Aaper. Poly(4-vinylpyrridine) (≥95%, M_W=60,000) was purchased from Sigma Aldrich. Ethanol (95%) used for cleaning slides was obtained from Pharmco Aaper. Reagent-grade absolute ethanol (>99.5%) from Aldrich was used for preparing 2% poly(4-vinylpyridine) solutions.

3.2 Equipment and Instrumentation

The fluorometer used in open atmosphere was a Perkin-Elmer LS-55. An ultraviolet visible extinction spectrometer, also used in the open atmosphere, is a product of Agilent Technolgies, model# 8453A. A VAC Vacuum Atmospheres glovebox, model MO-40-2H-SSG, operating with argon atmosphere was used to both make samples and perform most fluorescence measurements. A homemade fluorescence apparatus was utilized for fluorescence data collection, an image of which is shown in **Figure 7**. A 532 nm class IIIB laser was obtained from Shaan'xi Richeng Technology Development Co. LTD with a total output power capacity of 200 mW. The laser was directed through a

neutral density filter of OD 1, a product of Thor Labs. During measurements, the laser power was constantly monitored by a meter, a product of Thor Labs, model# PM100D.

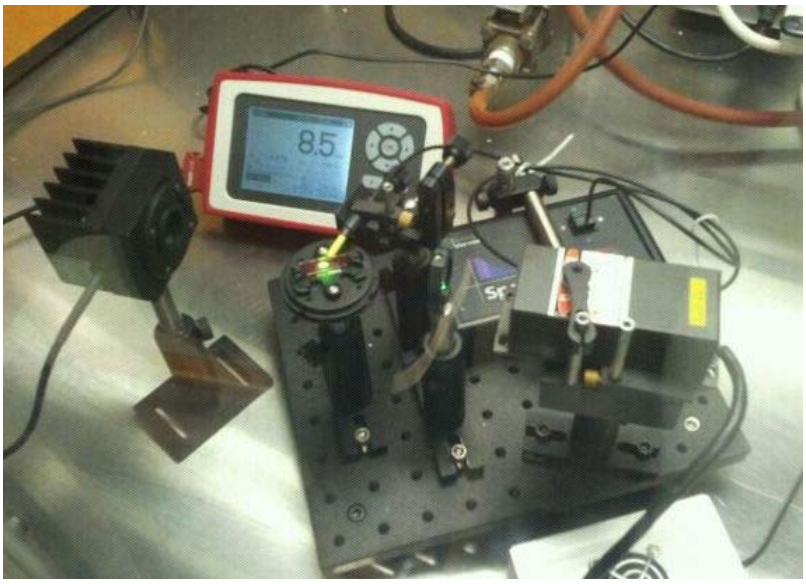

Figure 7: An image of the fluorescence apparatus within a glovebox.

The fluorescence is received by a fiber optic placed within close proximity to the sample slide. The fiber optic transmits the fluorescence to a portable spectrometer, a Vernier Spectrovis Pro, that is inside the glovebox and the results are displayed on an outside laptop via LoggerPro software. The fiber optic, a product of Ocean Optics, was adjusted vertically and horizontally while measuring a slide coated with plain P3HT, i.e. a P3HT film without underlying silver nanoparticles, to determine the optimal positioning and remained stationary for all future experiments. P3HT slides were prepared by spin-coating with a TC100 Spin-Coater from MTI Corporation. A KLA Tencor Alpha-Step IQ Surface Profiler was used for polymer thickness measurements. Electron microscopy was performed on a Hitachi HD2000 scanning transmission electron microscope

operating at 200 kV. Electron microscope samples were prepared by drop-casting particle suspensions onto formvar-coated copper grids from Electron Microscopy Sciences. Silver concentration was determined with a Perkin Elmer Optima 4100DV inductively-coupled plasma optical emission spectrometer (ICP-OES). Plasma-etching was carried out with a PDC-32G plasma cleaner by Harrick Plasma.

3.3 Synthesis of Silver Nanoparticles

The synthesis of silver nanoparticles utilized for this study occurs via the hydrogen reduction of silver (I) oxide in water.[65] This process is described by the chemical reaction shown in **Equation 1**. Approximately 3 g of silver oxide were added to a 5 L, 3-necked, Pyrex, round-bottomed flask and stirred with approximately 3 L of nanopure water.

$$Ag_2O\ (aq) + H_2\ (g) \rightarrow 2Ag^0\ (s) + H_2O\ (l) \qquad \textbf{Eq. 1}$$

The vessel was sealed and heated to 70°C before the hydrogen gas was applied at a pressure of 10 psi above atmosphere. The progress of the colloid formation was monitored by withdrawing aliquots of the suspension and analyzing them via UV-vis. The initiation of the formation of silver nanoparticles becomes apparent as the contents of the vessel begin to turn yellow after the addition of hydrogen gas. As particles increase in size, the suspension becomes a muddy green as the plasmon resonance shifts to longer wavelengths and scattering becomes the dominate plasmon relaxation mechanism. The reaction may be stopped at any time by the release of the hydrogen gas and yields crystalline silver particles. Therefore, particle size was varied simply by the adjustment of

the reaction time and was estimated via the wavelength of the maximum extinction observed at the dipole resonance mode and comparison to values previously established.[66] The apparatus used to prepare silver nanoparticles is shown in **Figure 8.**

Figure 8: The apparatus used to prepare silver nanoparticles consisting of a 5 L, three-necked, Pyrex, round-bottom flask in a heating mantel with gas valve, thermometer, and condenser.

Eight nanoparticle suspensions with different nanoparticle diameters were produced and studied for this project. Particle sizes were validated through imaging with electron microscopy conducted at Clemson University. This reaction, originally

described by Evanoff and Chumanov,[65] produces monodisperse, spherically-shaped particles, although rods and plates are also produced. Silver rods and plates are also produced in this reaction in addition to the spherical particles. Rods and plates present in the colloid were mostly removed by filtration through 0.45 and 0.22 μm filters. Centrifugation at 108 x *g* for 8 hours at 6°C is used to increase the colloid concentration, or optical density. The silver produced is not perfectly spherical and possesses facets as a result of the crystallinity. An example electron microscopy image of particles used during this experiment is shown in **Figure 9**.

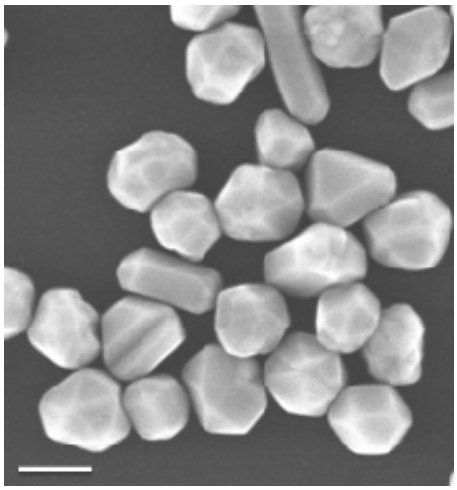

Figure 9: SEM image of silver nanoparticles. Scale bar represents 100 nm.

3.4 Sample Slide Preparation

The silver colloid was applied in varying concentrations to glass slides modified with poly(4-vinylpyridine) (PVP) to provide particle adhesion.[67] Soda-lime glass slides were cleaned by sonicating in alcohol followed by plasma etching. Slides were then

modified by placing them in vials of a 2% PVP in ethanol solution and agitating for several hours. The PVP solution was prepared by adding an appropriate amount of the polymer to ethanol, heated slightly, and stirred until all PVP dissolved. Each slide was rinsed with ethanol and water to remove excess PVP, dried with nitrogen gas, and heated in an oven at 80 °C for approximately one hour to anneal the polymer.

Suspensions of varying silver concentrations were made and adhered to the PVP surface by overnight immersion and placement on a rotator. After thorough coating, each slide was dried with nitrogen gas and the film was removed from one side of the slide with a cotton-tipped applicator so as to eliminate extinction from more than one layer of silver. All silver-coated glass slides were stored in 18.2 MΩ water if not immediately used. The slides were then placed on a spin-coater and the polymer applied to the surface. Typically, a 10 mg/mL solution of P3HT in chloroform was prepared and a volume of 100 μL was spin-coated onto the silvered side of the glass at varying speeds of 2,500, 3,500, and 4,500 RPM. The speed at which the film is cast typically directly correlates to its thickness. For example, polymer spun at a lower speed should produce a thicker film than polymer spun at a higher speed. The polymer layer thickness is an important aspect to consider while attempting fluorescence enhancement to determine the optimal ratio between silver nanoparticles and enhanced material. The thickness of the polymer layer was verified via contact profilometry, which was conducted at Clemson University.

After coating with P3HT, samples were placed on a slide holder and a 532nm laser was directed at the back of the glass slide so as to excite the silver before the P3HT. The fluorescence was observed via the LoggerPro software, which allowed for variance

of the integration time in milliseconds, number of spectra to average per measurement location, and emission wavelength range in nanometers. All analysis performed in this study included the ensemble averaging of five fluorescence spectra over a wavelength range of 540-900 nm. Sample time was kept at a constant 100 ms for all pure P3HT slides but was varied from 40 to 100 ms for P3HT/silver slides in order to produce a measureable spectrum considering enhanced fluorescence generated intense bands in some instances. However, all variance in sample time and its effect on overall EF was accounted for during final data analysis.

Three sample slides were prepared for each set of OD, particle size, and polymer layer thickness and fluorescence was measured at five locations across each sample to account for fluorescence variance across the films. Data produced by pure P3HT was analyzed by averaging fluorescence values across the slide and normalization of the sample time used. For the P3HT/silver samples, fluorescence across each slide was averaged followed by the averaging of all three samples. Integration time was also normalized to 1 s. Each spectrum was integrated from 600-800 nm and the area under the Ag/P3HT spectrum was divided by the corresponding plain P3HT spectrum to determine an EF value.

CHAPTER FOUR: RESULTS AND DISCUSSION

4.1 Exploratory Studies

Early work in this project showed an increase of fluorescence of the polymer when coupled with silver nanoparticles. Samples consisting of plain P3HT (with no underlying silver nanoparticles) and P3HT coupled with silver were prepared on substrates of PVP-coated glass slides. Each was analyzed via a Perkin Elmer LS-55 fluorometer and produced data such as that displayed in **Figure 10.**

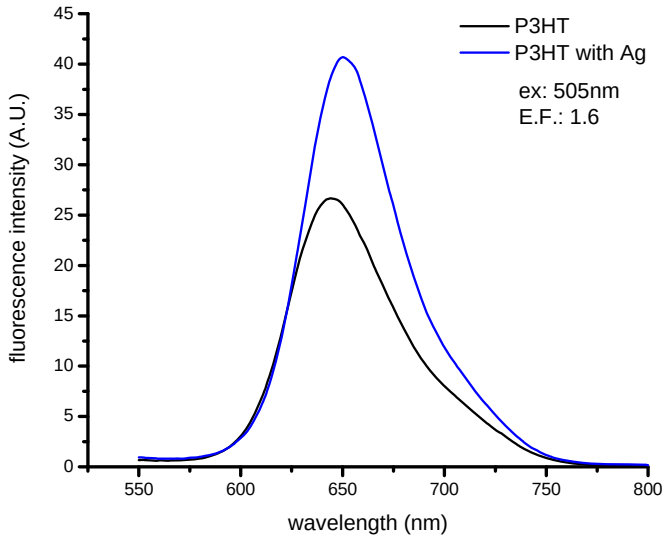

Figure 10: Fluorescence data of P3HT and silver-P3HT composite films. The films were excited at 505 nm, the absorption maximum for P3HT.

The wavelength chosen for excitation was 505nm, corresponding to the absorption maximum of P3HT. Enhancement results were considerably lower than anticipated, cf. **Figure 10**, which was attributed to the rapid degradation of the polymer in air as well as the particular measurement restrictions within the LS-55. In **Figure 11**, the photodegradation of a plain P3HT film is shown.

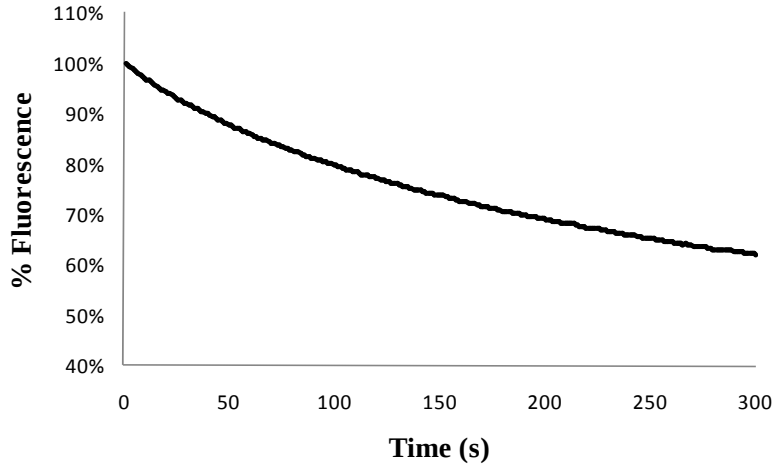

Figure 11: P3HT degradation as measured with the LS-55 in open atmosphere.

A rapid degradation of the fluorescence signal was apparent as the same sample was measured over time. Fluorescence collections with the LS-55 were considered inefficient considering the fluorometer design limits the manner in which the samples are measured. In this case, the incident light reaches the polymer before the silver. Consequently, polymer excitation occurs prior to that of the silver. Ideally, the silver should be excited first to ensure that the maximum amount of forward Mie scattering is directed into the polymer film. We believed that results obtained from the LS-55 relied

mostly on the small amount of Mie back-scattering into the polymer surface, rather than the far larger forward scattering field.

The problems of polymer degradation and measurement geometry were corrected by utilizing a glovebox, which housed a homebuilt laser apparatus, described previously. Our design directs the laser at the back of the glass slide and therefore excites the silver before the polymer layer. Performing experiments within the glovebox, which is under an argon atmosphere, also lessens the potential of P3HT to oxidize and degrade (see section 4.3).

4.2 Instrument and Measurement Comparability

A series of experiments were carried out in order to resolve the optimal method in which to measure sample slides. One study focused on determining the comparability between the two fluorometers by measuring the fluorescence of plain P3HT samples inside of the glovebox as well as in open atmosphere. A 1 mg/mL solution of P3HT in chloroform was prepared and spin-coated onto PVP-coated glass slides. Coatings of the P3HT were applied to five slides at speeds of 1000-5000 RPM, each producing polymer layers of varying thicknesses. The fluorescence of each slide of a varying thickness was measured using both the Perkin-Elmer LS-55 and the home-built fluorometer. At this time, the fluorescence analysis within the glovebox was carried out using a battery-operated laser with a wavelength of 532 nm. Performing the sample experiment both in ambient conditions, as well as under an inert atmosphere, allowed for the evaluation of comparability between instruments and consistency of results. While both manners of measurement show comparable fluorescence results, there exists a distinct difference in the resulting P3HT spectrum. The fluorescence of P3HT in the open atmosphere yields a

major peak at ca. 640 nm with a broad shoulder at ca. 710 nm, as shown previously in **Figure 10**. In contrast, fluorescence measured in the glovebox results in a dramatic increase in intensity of the lower energy band. It is well known that the higher energy band of the P3HT film spectrum results from monomer-like emission while the low energy band is due to π-stacked lamellar structures within the film, i.e. excimer emission.[68]

The relative ratios of the bands can be influenced by factors including the degree of regioregularity of the hexyl side chains or even the solvent from which the polymer is cast.[69, 70] **Figure 12** shows a comparison of plain P3HT and Ag/P3HT films measured in the LS-55 and glovebox fluorometer. The spectra have been normalized to the high energy peak of each film system. Surprisingly, the exact same films display significant differences in the relative heights of the high and low energy bands. Most likely, the spectral differences are due to differences in the polarization of the source. Using polarization filters in the LS-55 had significant impact on the relative ratio of the bands.

For measurements made in the LS-55, the sample chamber was rapidly flushed with N_2 (g) to limit oxidative degradation during data collection. The slight red-shifting (7 nm) that is evident when comparing the higher-energy emission bands collected in the glovebox to those collected in the LS-55 is most likely due to changes in medium refractive index, as the glovebox atmosphere was argon (as compared to nitrogen in the LS-55) at typically 1.5 – 3 torr above ambient pressure. Likewise, refractive index changes are the likely cause the modest red-shift of 3 nm that occurs when comparing Ag/P3HT films to plain P3HT films.

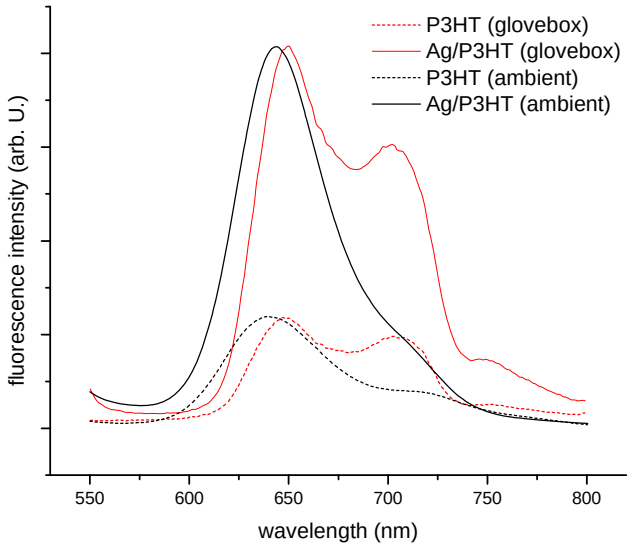

Figure 12: Fluorescence measurements of plain P3HT and Ag/P3HT films with the LS-55 in open atmosphere (black) and inside the glovebox (red). Silver films were prepared from an OD 3 suspension of 118 nm particles. P3HT films were spin-cast at 3,500 RPM.

Also evident in the data presented in **Figure 12** is that the addition of the underlying silver particles disrupts the π-stacking of the P3HT. For the films measured in the glovebox, the ratio of the low energy to high energy band drops from 0.83 to 0.74 when silver is added to the film. Increasing particle size and concentration increases the amount of π-stacking disruption in the film. Fortuitously, a recent report by Mauer et al. has suggested that the high levels of π-stacking achieved by casting regioregular polymers do not equate to higher performing devices when compared to devices made from the disordered films of regiorandom polymers.[71] Those results suggest that in a device, plasmonic excitation enhancement will not be counteracted by negative impacts of film disorder.

Another experiment involved determining the consistency of measurements taken within the glovebox by measuring different P3HT slides of the same thickness and comparing resulting fluorescence data. In addition, multiple measurements were collected across a single slide to study how fluorescence varies across a film. Results showed considerable consistency when measuring several slides of the same thickness, but showed noticeable decrease in fluorescence when moving from the center of a slide to an edge as can be seen in **Figure 13.** However, the inconsistency among the slide has been accounted for by collecting the fluorescence measurements at five locations across the slide and determining an average fluorescence value.

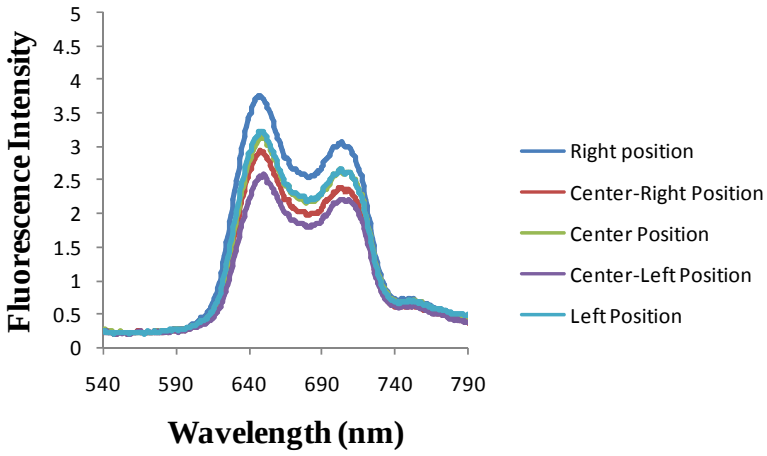

Figure 13: Fluorescence variance resulting from measurements taken from different locations across a sample slide.

A second experiment to ensure measurement consistency was performed in which P3HT was spin-cast at varying speeds onto PVP-coated glass. A 10 mg/mL solution of

P3HT in chloroform was prepared and 100 µL were added onto the PVP-coated side of the glass. The spin-coating speeds were varied between 1,000-5,000 RPM and measured within the glovebox. The samples were prepared and analyzed on separate days, and produced data that was inconclusive and yielded no noticeable correlation between spin-coating speed and polymer thickness, as shown in **Figure 14.**

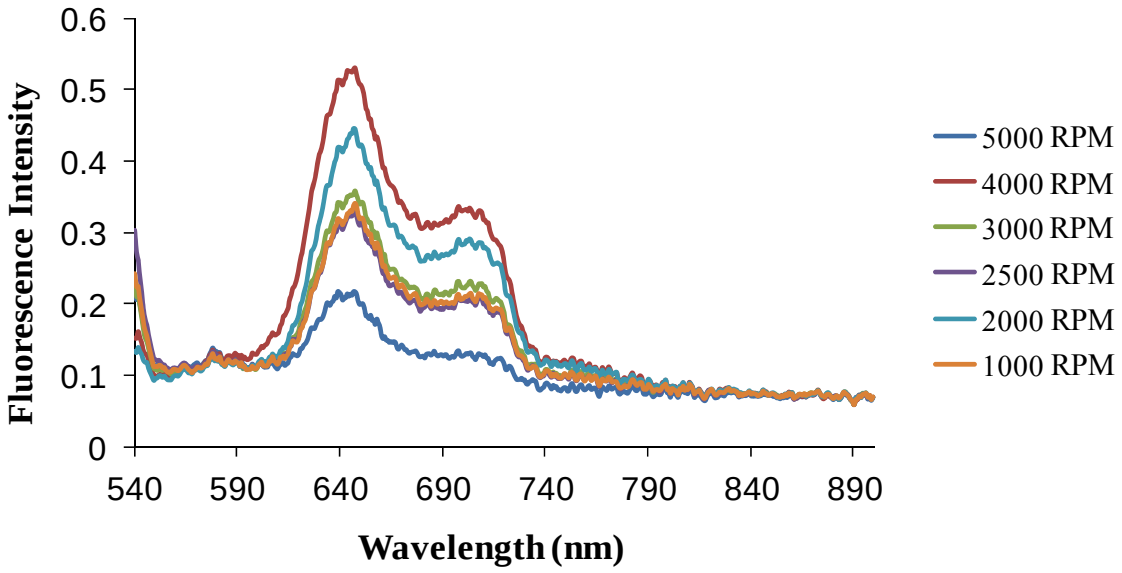

Figure 14: Fluorescence analysis within a glovebox of polymer slides prepared from spin-coating speeds of 1,000-5,000 RPM. Slides were prepared and analyzed on different days.

However, the same experiment was conducted in which the samples were prepared and analyzed on the same day. The data produced and displayed in **Figure 15** proved comparable to the expected results, which showed a direct correlation between spin-

coating speed and fluorescence, presumably based on polymer thickness. It was predicted that thicker films - those prepared by slower spin-coating speeds - would produce higher fluorescence peaks due to the greater capacity for exciton formation. The lack of correlation shown in the first experiment may be attributed to the degradation of the polymer or the effects of exposure to light.

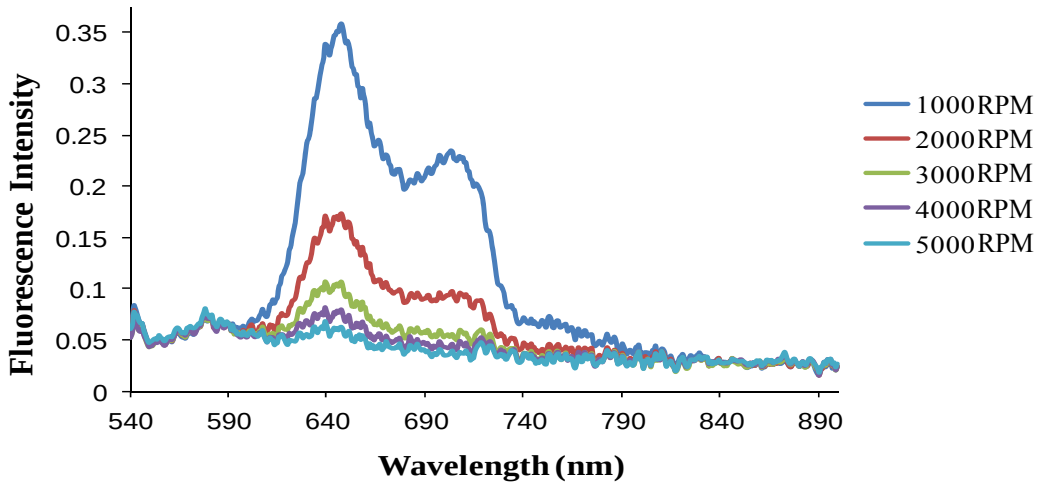

Figure 15: Fluorescence spectra of poly(3-hexylthiophene) cast at 1,000-5,000 RPM. Same day preparation and analysis.

4.3 Glovebox Conditions and Polymer Degradation

Another potential cause may be due to trace amounts of water and/or oxygen present within the glovebox. The detection method for these contaminants involves titanium tetrachloride and diethyl zinc, respectively. Each bottle was opened and observed for the production of smoke, indicating levels greater than approximately 5 ppm

of oxygen and 10 ppm of water. Concentrations below this level may still contribute to the degradation of the P3HT. Analysis of the polymer films in the open atmosphere also showed rapid degradation due to the exposure to the air, but considerably less within the glovebox. After the data in **Figures 14** and **15** were collected, however, the molecular sieves and oxygen-reducing catalyst in the glovebox circulation unit were changed. After several treatments of the new catalyst to heat in a reducing atmosphere, the catalyst should be able to maintain O_2(g) and H_2O (g) levels well below 1 ppm. Upon changing the catalyst, the films showed much better long term stability.

Continued exposure of the polymer to laser excitation, however, will cause photodegradation of the film, even in an inert atmosphere. A 3.6% photodegradation of a plain P3HT film with 300 s of constant laser exposure can be observed (**Figure 16a**). An identical study of the degradation of P3HT with underlying 118 nm silver particles also shows similar results with 3.4% fluorescence decay (**Figure 16b**). The measurement described above was performed six months after the films were cast. Fluorescence measurements of the films after storage were within the standard deviation of the original measurements of the freshly-prepared films. This result indicates that the inert atmosphere eliminates P3HT oxidation.

(a)

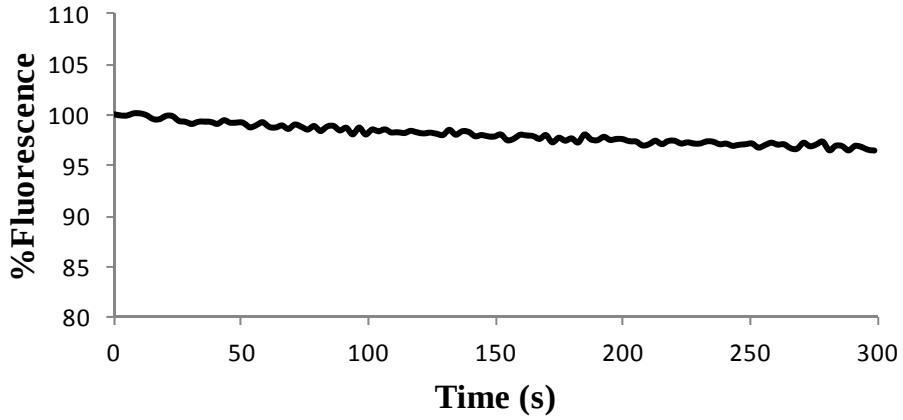

(b)

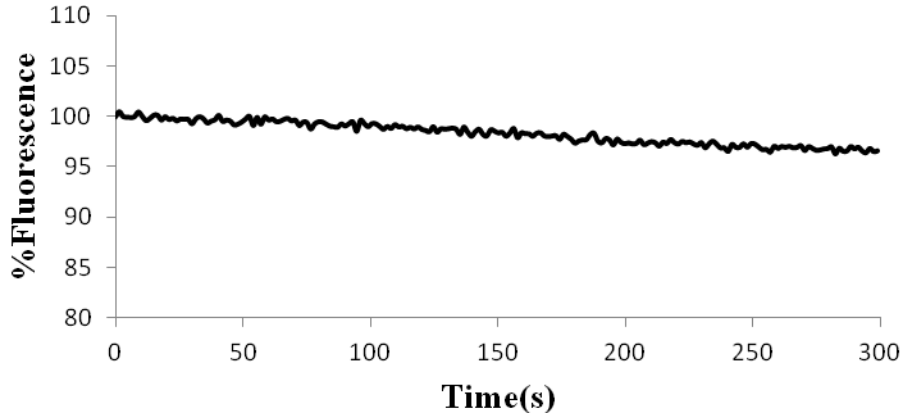

Figure 16: Stability of (a) plain P3HT film and of (b) a Ag/P3HT sample as measured in the glovebox.

To ensure maximum reliability, samples were made and measured on the same day to minimize oxidative degradation. Likewise, measurements of a particular film volume were completed in only a few seconds of laser exposure to minimize photodegradation. Difficulties arose in maintaining consistency in results due to fluctuations in supplied power. To ensure that the spectral decay occurred as a result of

P3HT degradation and not laser instability, an alternative laser was used with an AC power source and thermoelectric cooling to maintain a constant power output. As a result of exchanging lasers, a variety of experiments were carried out to ensure laser stability which include time studies on various samples which involve measuring fluorescence at a known point as a function of time. The 532 nm laser utilized for the collection of data produces a stable beam of ca. 20.0 mW, as determined via a power meter, with minimal fluctuation. For each experiment, the laser was allowed to stabilize for 20 min prior to data collection. From these preliminary studies, it was evident that the fluorescence equipment set up within the glovebox provided sample measurement with optimal consistency and minimal sample degradation.

4.4 Sample Measurement and Analysis

Based on the aforementioned experimentation, a valid standard operating procedure for the laser and best method for P3HT analysis was determined. It was concluded that sample analysis involved same-day sample preparation and analysis as well as averaging multiple data collections across a slide. LoggerPro measurements parameters included a set sample time of 100 ms for P3HT sample slides and varying sample time from 40-100 ms for P3HT/silver samples, depending on the height of the fluorescence peak. During data analysis, all integration times were normalized to a sample time of 1 s for comparable results. Emission spectra were collected from 540-900 nm and five spectra were averaged for each measurement.

The study involved preparing samples of P3HT slides by spin-coating at speeds of 2,500, 3,500, and 4,500 RPM without the presence of silver. These samples were measured immediately before analysis of samples with silver present prepared by equal

spin-coating speeds. This allowed for an immediate observation of enhanced fluorescence. The silver particle diameter was varied from 15-153 nm. Each sample was prepared from suspensions of ODs of 1, 3, and 5. Each sample has been measured in five locations across each slide. Analysis on various areas of the slide provided the ability to collect an average fluorescence of the polymer, as well as when the polymer is coupled with silver. To determine EF, the area under the silver/P3HT spectrum was divided by the area under the corresponding plain P3HT spectrum. Sample fluorescence results obtained from within the glovebox are displayed in **Figure 17.**

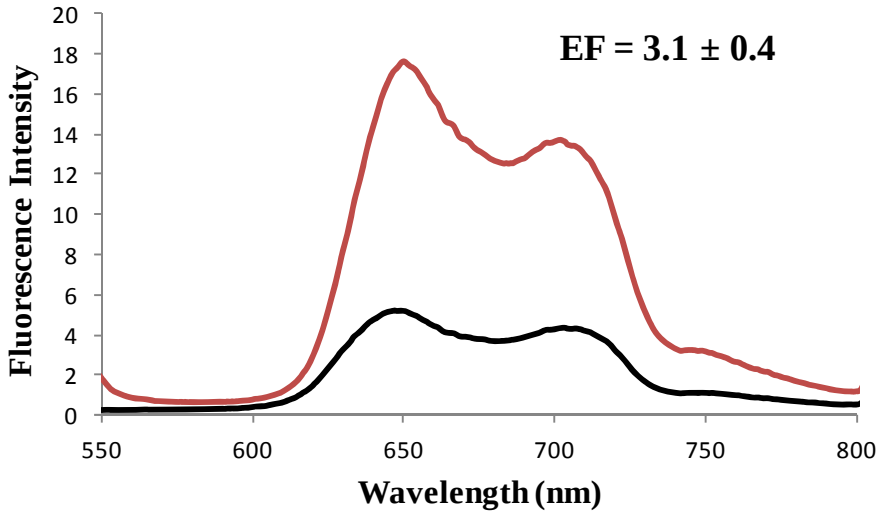

Figure 17: Fluorescence data obtained from a P3HT sample spin-cast at 3,500 RPM (black) and a sample of P3HT spin-cast at 3,500 RPM paired with 137 nm silver particles prepared from an OD 3 suspension (red).

4.5 Results and Discussion

Measuring the fluorescence of P3HT paired with eight silver suspensions of different sizes and concentrations yielded results that were somewhat inconclusive. Observing EF as a function of OD showed no discernable trend regardless of particle size or spin-coating speed. It was predicted that samples made of higher optical densities would lessen the enhancement factor due to particle coupling which occurs when nanoparticles are spaced closely together. **Table 1** shows enhancement factors generated during the study. The table is organized to show how EF is affected by variations in OD. Sets of ODs can be seen moving down the table and are separated by polymer spin-coating speeds.

Table 1: Collection of data representing EF of P3HT produced by varying silver optical densities on sample slides. The data is separated by spin-coating speed of the polymer and shows particle diameter increasing from left to right.

	Particle Diameter							
	15 ± 1nm	**54 ± 4nm**	**66 ± 4nm**	**107 ± 9nm**	**118 ± 8nm**	**121 ± 9nm**	**137 ± 11nm**	**153 ± 12nm**
OD 1	1.0 ± 0.0	1.3 ± 0.3	1.9 ± 0.1	1.4 ± 0.3	2.9 ± 0.2	2.2 ± 0.1	1.3 ± 0.1	3.1 ± 0.3
OD 3	0.9 ± 0.0	1.5 ± 0.1	1.8 ± 0.1	2.5 ± 0.2	3.3 ± 0.3	3.3 ± 0.3	3.3 ± 0.2	4.9 ± 0.2
OD 5	0.8 ± 0.0	1.4 ± 0.1	1.6 ± 0.1	2.5 ± 0.1	3.5 ± 0.1	3.2 ± 0.1	3.2 ± 0.2	3.4 ± 0.1
OD 1	0.9 ± 0.0	2.0 ± 0.2	1.9 ± 0.2	1.3 ± 0.1	3.3 ± 0.5	1.9 ± 0.2	1.4 ± 0.2	3.3 ± 0.3
OD 3	0.9 ± 0.0	1.3 ± 0.1	1.9 ± 0.1	2.9 ± 0.1	3.0 ± 0.2	3.2 ± 0.2	3.1 ± 0.4	3.1 ± 0.1
OD 5	0.9 ± 0.0	1.4 0.1	1.8 ± 0.1	2.9 ± 0.0	3.5 ± 0.5	3.4 ± 0.2	3.5 ± 0.0	3.3 ± 0.2
OD 1	0.9 ± 0.0	1.6 ± 0.2	1.8 ± 0.2	1.5 ± 0.1	3.4 ± 0.1	2.2 ± 0.2	1.4 ± 0.2	3.9 ± 0.3
OD 3	0.9 ± 0.1	1.5 ± 0.4	1.8 ± 0.1	2.3 ± 0.3	3.7 ± 0.2	2.9 ± 0.1	3.5 ± 0.3	3.5 ± 0.2
OD 5	0.8 ± 0.1	1.6 ± 0.1	1.5 ± 0.1	3.3 ± 0.1	3.8 ± 0.2	3.2 ± 0.1	3.3 ± 0.6	3.8 ± 0.1
		2,500 rpm		**3,500 rpm**		**4,500 rpm**		

Within a few sets of data there is a decrease in EF with higher OD which is consistent with the theory of particle coupling. However, the majority of data yields no distinguishable correlation between variance in OD, regardless of particle diameter or the thickness of the polymer layer. An explanation for the lack of correlation may stem over the lack of control over the amount of polymer that is spin-cast onto the substrate as the amount of silver increases. Contact profilometry results show that film thickness changes unpredictably in Ag/P3HT films. Adhesion of the P3HT is likely quite different on Ag compared to PVP-coated glass. As a result, higher OD films may contain significantly less P3HT. The true concentration-dependent EF is difficult to discern without a method to standardize against P3HT concentration. Future studies in this area might include placing an internal standard in the P3HT solution or developing a protocol to disperse silver particles in the P3HT solution prior to spin coating.

After obtaining the results discussed above, additional experiments were conducted to observe the effects from slides that were prepared from higher concentrated silver suspensions to more fully understand the effect of silver coupling. Slides were prepared from 118 nm silver nanoparticle suspensions with OD of 50 and 100 to further examine the effect of coupling on polymer fluorescence. Each slide was coated with P3HT at a spin-coating speed of 3,500 RPM and compared to spectra produced from OD 1, 3, and 5. Results are shown in **Figure 18**.

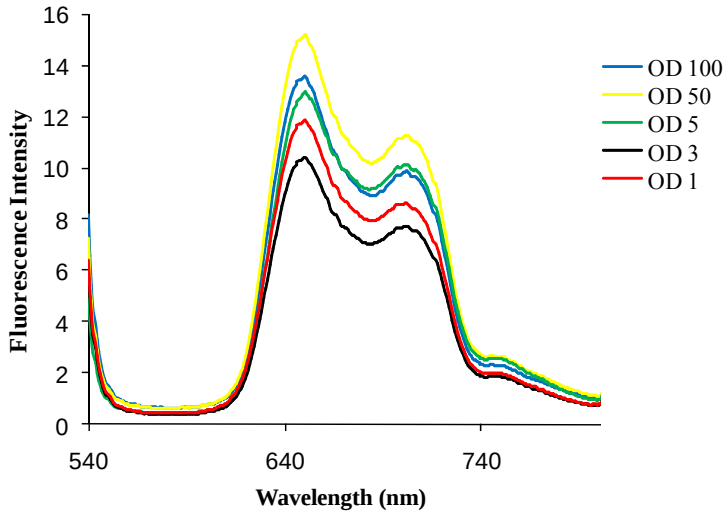

Figure 18: Spectra of P3HT spin-coated at 3,500 RPM onto 118 nm silver prepared from ODs of 1, 3, 5, 50, and 100.

It was anticipated that fluorescence enhancement would decrease significantly with higher ODs considering the mainly absorptive resonance particles exhibit when particles in 2D arrays become quadrupole-coupled [72, 73]. The slides prepared from suspensions of OD 50 and 100 were expected to be highly coupled and would therefore yield significantly lower values than a sample prepared from an OD 1 suspension. However, fluorescence intensities produced with the slides of high ODs remained comparable to those observed previously with samples of OD 1, 3, and 5. The results suggest that the addition of P3HT to the silver surface is altering the manner in which the particles extinguish light, perhaps at least partially disrupting the quadrupolar coupling.

To explore this possibility, slides were prepared from OD 1, 5, and 100 suspensions using 118 nm diameter particles. The extinction of the silver films were

measured using UV-Vis and each sample's extinction was measured three separate times: while the slides were in water, after drying with nitrogen gas, and also when coated with P3HT at a spin-coating speed of 3,500 RPM. In the latter case, the spectrum of plain P3HT absorbance was subtracted from the spectrum of each P3HT/silver film extinction. To perform the subtraction, spectra were first normalized at both 320 nm and 1100 nm. At 320 nm, both P3HT and silver have a spectral minimum while the extinction from either at 1100 nm should be zero. The results can be seen in **Figure 19.**

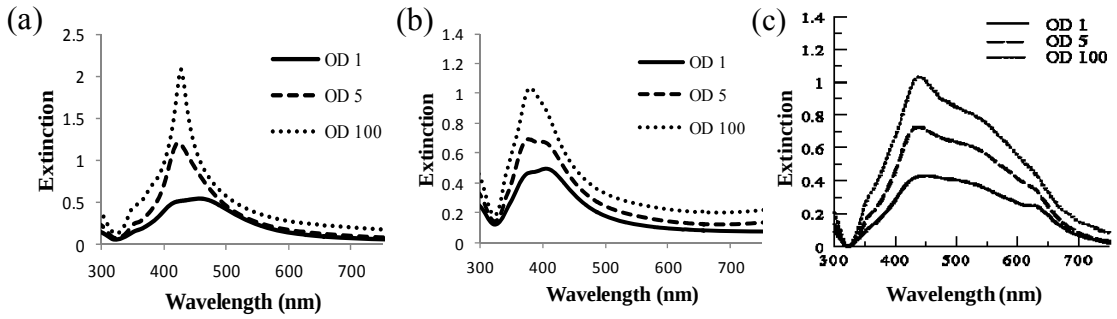

Figure 19: Extinction spectra produced from slides prepared from ODs 1, 5, and 100 of 118 nm silver particles. UV-Vis measurements were obtained from slides (a) in water, (b) after drying with nitrogen gas, (c) of polymer-coated silver from which the absorption spectrum of plain P3HT was subtracted.

It has been previously reported that approximately 100 nm silver nanoparticles exhibit distinct spectra when coupled and uncoupled; phenomena that are influenced by interparticle spacing.[72] Therefore, a 118 nm silver suspension was chosen for comparability in the study presented in **Figure 19**. Suspensions of these particles exhibit

a spectrum of two peaks; a broad dipole band centered at 522 nm, and a second, higher energy band centered at a 425 nm.[72] The 425 nm band is the result of quadrupolar electronic oscillations within the particle due to phase retardation of the incident light. When plasmon resonances are excited in particles larger than about 50 nm, the plasmon excitation frequency becomes somewhat comparable to particle size such that the particles' conduction electrons experience an inhomogeneous electric field, resulting in more complex oscillations of the electrons such as the quadrupole, octupole, or hexadecapole resonance.[35] When particles in a film become closely spaced, the non-radiative electric fields that exist during individual particle plasmon resonances overlap with those of their neighbors. The interaction of electric fields gives rise to a coupled plasmon resonance across the film. Malynych and Chumanov have shown that symmetry dictates that the coupled resonance in a 2D array be mainly quadrupolar in nature.[72] This phenomenon is evident when comparing the extinction spectrum of the 118 nm particle suspension shown in **Figure 5** with those of the particle films presented in **Figure 19a**. In a film prepared from an OD 1 suspension, the interparticle spacing is large enough that the film spectrum resembles that of the suspension with slight shifts in each resonance resulting from the change in the dielectric function of the particles' surrounding medium. As suspension OD increases, coupling clearly increases as evident from the disappearance of the dipole plasmon maximum and enhancement of the quadrupole resonance at 436nm. Upon drying the films in **19b**, the quadrupole peak blue-shifts due to the decrease in the dielectric function of the particles' surrounding medium. In **19c**, it is apparent that the addition of P3HT to the silver film is causing the plasmon resonance to decouple and is shown by the slight reemergence of the dipole

peak. In each OD, the dipole and quadupole resonance are clearly visible as a broad band and a distinctly sharper peak, respectively. At this time it is difficult to determine what is causing the loss of coupling. Assuming that the P3HT casting is not causing a large amount of particles to be removed from the film, then it would seem that the higher refractive index of the polymer is decreasing the non-radiative field decay length enough to decouple. It is possible though that spin-casting is removing enough particles to increase particle spacing to a point where coupling does not exist. In the future, an interesting study would be to determine if the interparticle spacing under the P3HT film by performing scanning electron microscopy with a backscattering detector such that the particles could be imaged under the film.

Upon studying the generated data, there also appeared to be no correlation between spin-coating speed, or polymer thickness, and the overall effects on fluorescence enhancement, as shown in **Table 2.** It was predicted that a particular thickness of the polymer layer would provide an ideal ratio of fluorescent material to the nanoparticles. Films of thinner thicknesses exhibit reduced electron/hole recombination while thicker films possess the ability to generate more excitons. The table is organized to show how EF is affected by polymer spin-coating speed, which should correlate to the thickness of the particular layer. Sets of spin-coating speeds can be seen moving down the table and are separated by optical densities. Particle diameter, as in the previous table, increases when moving right across the table.

Table 2: Collection of data representing EF of P3HT produced by varying polymer spin speed on sample slides. The data is separated by spin-coating speed of the polymer and shows particle diameter increasing from left to right.

	Particle Diameter							
	15 ± 1nm	**54 ± 4nm**	**66 ± 4nm**	**107 ± 9nm**	**118 ± 8nm**	**121 ± 9nm**	**137 ± 11nm**	**153 ± 12nm**
2,500	1.0 ± 0.0	1.3 ± 0.3	1.9 ± 0.1	1.4 ± 0.3	2.9 ± 0.2	2.2 ± 0.1	1.3 ± 0.1	3.1 ± 0.3
3,500	0.9 ± 0.0	2.0 ± 0.2	1.9 ± 0.2	1.3 ± 0.1	3.3 ± .05	1.9 ± 0.2	1.4 ± 0.2	3.3 ± 0.3
4,500	0.9 ± 0.0	1.6 ± 0.2	1.8 ± 0.2	1.5 ± 0.1	3.4 ± 0.1	2.2 ± 0.2	1.4 ± 0.2	3.9 ± 0.3
2,500	0.9 ± 0.0	2.0 ± 0.2	1.8 ± 0.1	2.5 ± 0.2	3.3 ± 0.3	3.3 ± 0.3	3.3 ± 0.2	4.9 ± 0.2
3,500	0.9 ± 0.0	1.3 ± 0.1	1.9 ± 0.1	2.9 ± 0.1	3.0 ± 0.2	3.2 ± 0.2	3.1 ± 0.4	3.1 ± 0.1
4,500	0.9 ± 0.1	1.5 ± 0.4	1.8 ± 0.1	2.3 ± 0.3	3.7 ± 0.2	2.9 ± 0.1	3.5 ± 0.3	3.5 ± 0.2
2,500	0.8 ± 0.0	1.4 ± 0.1	1.6 ± 0.1	2.5 ± 0.1	3.5 ± 0.1	3.2 ± 0.1	3.2 ± 0.2	3.4 ± 0.1
3,500	0.9 ± 0.0	1.4 ± 0.1	1.8 ± 0.1	2.9 ± 0.0	3.5 ± 0.5	3.4 ± 0.2	3.5 ± 0.0	3.3 ± 0.2
4,500	0.8 ± 0.1	1.6 ± 0.1	1.5 ± 0.1	3.3 ± 0.1	3.8 ± 0.2	3.2 ± 0.1	3.3 ± 0.6	3.8 ± 0.1

OD 1 **OD 3** **OD 5**

There is no distinguishable trend relating spin-coating speed to fluorescence EF. Contact profilometry on a collection of slides confirmed that there exists an inconsistency in spin-coating speed of the polymer and the resulting thickness. It has since been determined that the current method of applying the P3HT to the silver-coated slide surface lacks controllability over the manner in which the polymer lies over the particles. Considering spin-coating appears to be an ineffective means of applying P3HT to sample slides, the future direction of this research may studying other means of depositing the polymer onto the sample slide such as dip-coating, a process involving the submersion of a substrate directly into the coating material. Film thickness can be controlled by varying the viscosity of the solution as well as the withdrawing speed, although solvent evaporation may be a potential drawback.[74] Other options include pursuing attempts at

spray coating the polymer to the silver surface, a process in which solution droplets are applied to a structure via spray gun. This method allows controllability of the surface texture and reportedly generates reproducible and uniform results.[75] Reports in other studies have also mentioned the incorporation of a nanoparticle suspension directly into a polymer solution before application to a substrate[76] and may serve as a future direction in this research for correcting the issues associated with polymer spin-casting.

The distinguishable trend exhibited during this study was between particle size and enhanced fluorescence, as can be observed from **Tables 1** and **2**. In most instances, the correlation showed that EF increased with larger particle sizes and occurred independently of particle concentration and spin-coating speed. This outcome may be the result of the manner in which particles extinguish light, a feature that is dependent on particle size. This trend aligns with the original hypothesis that larger particles would provide greater enhancement due to their ability to scatter more light than smaller particles.

The trend described above is perhaps more impressive when considering that an OD 3 suspension of 15 nm particles contains 38 times more particles than a suspension of 137 nm particles with the same OD.[66] To gain a better understanding of the effect of particle size on enhancement, a value termed particle enhancement was determined by normalizing EF to the total number of particles within the laser excitation spot. Number of silver particles was calculated by measuring the total amount of silver on a slide by ICP-OES. Slides were exposed to HNO_3 (*aq*) to dissolve the silver particles. The delaminated, oxidized P3HT was removed by filtration with 0.45 μm nylon membranes.

Following determination of Ag^+ concentration, a series of calculations were

performed to determine the number of silver particles on each slide. The calculation uses the assumptions of standard molar volume of silver atoms and that the silver particles are evenly distributed across the face and sides of the glass substrate. For comparison to EF, the number of particles within the laser spot was calculated. EF was divided by this estimated number of particles to calculate particle enhancement. The horizontal error bars represent deviations associated with particle diameter. The vertical error bars account for error associated with ICP-OES measurements and fluorescence deviations.

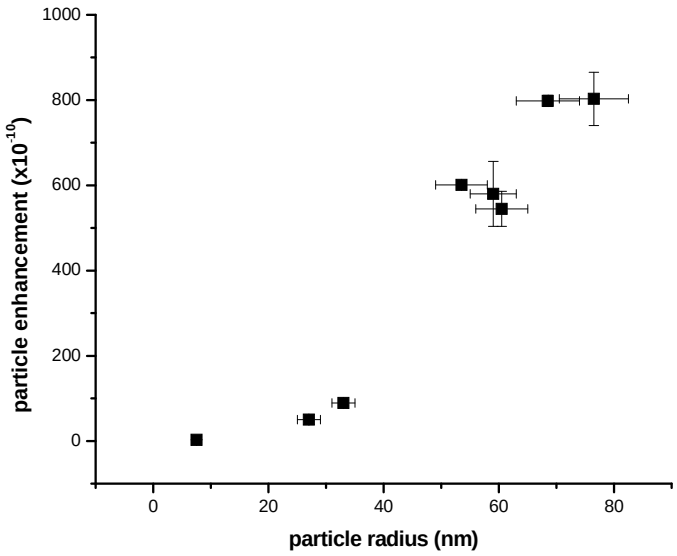

Figure 20: Particle enhancement as a function of particle radius.

In **Figure 20**, particle enhancement as a function of particle radius is shown for each particle size. Samples used for this study all contained silver films prepared from OD 5 suspensions and P3HT films spin cast at 3500 RPM. The vertical error bars were calculated from the sum of percent relative standard deviations of the ICP-OES concentration measurement and EF calculation. The data in **Figure 20** clearly

demonstrates the strong dependence of EF on particle size. Larger particles provide a two order of magnitude improvement in EF as compared to the smallest particles used in this study – an important result considering the lack of present literature reporting fluorescence enhancement generated from particles of this size range.

While the general trend is clear, some inconsistency is evident when comparing particle enhancements of particles of similar radii. The method of particle concentration determination is prone to some error based on assumptions made. For example, total monodispersity of the particles is assumed and non-spherical particle shapes are ignored, similar particle adhesion to the face and sides of the glass substrates is assumed, and damage made to the film during measurement is disregarded. Nevertheless, particle enhancement as determined by ICP-OES reveals the strong correlation between particle size and enhancement.

Analysis of scanning electron microscopy images would provide a more accurate measurement of particles under the P3HT film. Unfortunately, charging of the P3HT film during image acquisition inhibits resolution of the underlying particles with a standard detector. In the future, analysis of the remaining films with a nondestructive method such as scanning electron microscopy with a back scatter detector should provide a more accurate particle count and thus a more accurate determination of particle enhancement.

CHAPTER FIVE: CONCLUSION

The studies conducted in this project have provided future opportunities within the lab to continue optimizing maximum fluorescence enhancement parameters as well as the eventual application to organic PVDs. It has been determined that incorporating silver nanoparticles onto the polymer surface does increase the generated fluorescence and that the size of the nanoparticle also significantly contributes to a higher enhancement factor. This enhanced fluorescence is the result of an increased number of excitons formed within the polymer and will, ideally, translate into higher efficiency within a device. The experimentation performed during this project has contributed to the determination of a set protocol for sample preparation, analysis, and measurement conditions, as well as a better understanding of how each parameter may affect efficiency enhancement. Future research may focus on further optimizing the parameters studied during this project as well as the eventual application towards enhancing the power conversion efficiency within organic PVDs.

Upon completion of this project, fluorescence enhancement of the organic polymer P3HT has been attained by placing silver nanoparticles of various sizes and concentrations within close proximity to a polymer layer. At the end of the study, several important goals were achieved:

1) A reliable method to reproducibly make and measure Ag/P3HT films was established, including the fabrication and testing of a fluorescence spectrometer.

2) The effect of particle size on fluorescence enhancement was determined. EF increased with increased particle size, although true quantification is difficult without a true concentration of Ag particles within the film.
3) OD and spin-coating speed were shown to have little effect on EF within the ranges tested. Contrary to the initial hypothesis, interparticle coupling exhibited by silver particle films did not have a negative impact on EF because addition of P3HT broke the coupling.

Future studies in this research area include the following:

1) Using silver-silica core-shell particles. In typical SEF, dielectric barrier layers are used to minimize quenching. The ultrathin silica layers discussed in Chapter One might be useful for both minimizing quenching and providing electrical isolation of the particles in a device.
2) Determining a methodology for either controlling or accurately measuring concentration of silver particles in the P3HT film. As discussed in Chapter Four, SEM with a backscattering detector should provide the necessary penetration depth to image the particles or perhaps sectioning a Ag/P3HT film with focused ion beam lithography prior to electron microscopy to remove the top-most P3HT. Synthesizing a protective layer around the silver (such as the silica layer described above) might allow Ag particles to be dispersed in a polymer solution without particle oxidation and aggregation. Such dispersion would allow for better control of particle concentration within the film and perhaps better control of film thickness.

3) Determining a better methodology for film deposition. Although spin-casting is the most widely used method for device fabrication, it was found that this type of deposition onto a rough surface lead to poor control of film thickness. Alternative methods of film-casting such as those discussed in Chapter Four may yield better results. Likewise, as discussed above, dispersal of the Ag into the P3HT solution prior to casting may also yield better results.

CHAPTER SIX: WORKS CITED

1. Logothetidis, S. Flexible Organic Electronic Devices – Materials, Process, and Applications. *Mater. Sci. Eng., B* **2008,** *152,* 96-104.
2. The solar spectrum is adapted from the 2000 ASTM Standard Extraterestrial Spectrum Reference E-490-00. http://rredc.nrel.gov/solar/spectra/am0/ASTM2000.html. Date Last Accessed: 11 March 2012.
3. Moule, A., Allard, S., Kronenberg, N. Effect of Polymer Nanoparticle Formation on the Efficiency of Polythiophene Based "Bulk-Heterojunction" Solar Cells. *J. Phys. Chem. C* **2008**, *112*, 12583-12589.
4. Chen, F., Wu, J., Lee, C. Plasmonic-Enhanced Polymer Photovoltaic Devices Incorporating Solution-Processable Metal Nanoparticles. *App. Phys. Lett.* **2009**, *95*, 013305.
5. Petzold, S., Wang, C., Khazaal, A., et al. Conjugated Polymer Photovoltaic Solar Cells: Manufacturing and Increasing Performance. *Plastics Engineering Magazine* **June 2010**. 26-32.
6. Shen, H., Bienstman, P., Maes, B. Plasmonic Absorption Enhancement in Organic Solar Cells with Thin Active Layers. *J. App. Phys*. **2009**, *106*, 073109.
7. Spanggaard, H., Krebs, F. A Brief History of the Development of Organic and Polymeric Photovoltaics. *Sol. Energ. Mater. and Sol. C* **2004**, *83*, 125–146.
8. Borsenberger, P., Weiss, D. Organic Photoreceptors for Imaging Systems, Marcel Dekker, New York, **1993**.
9. Bube, R. Photoconductivity of Solids. *Physics Today* **1960**, *14*, 54.
10. Tang, C. Two-Layer Photovoltaic Cell. *Appl. Phys. Lett*. **1986**, *48*, 183–185.
11. Kim, J., Kim, K., Ko, S., et al. Optimum Design of Ordered Bulk Heterojunction Organic Photovoltaics. *Sol. Energ. Mater. and Sol. C* **2011**, *95*, 3021–3024.
12. Mazhari, B. An Improved Solar Cell Circuit Model for Organic Solar Cells. *Sol. Energ. Mater. and Sol. C* **2006**, *90*, 1021–1033.
13. Ojala, A., Burckstummer, H., Stotle, M., et al. Parallel Bulk-Heterojunction Solar Cell by Electrostatically Driven Phase Separation. *Adv. Mater*. **2011**, *43*, 5398-5403.
14. Walker, B., Han, X., Kim, C., et al. Solution-Processed Organic Solar Cells from Dye Molecules: An Investigation of Diketopyrrolopyrrole:Vinazene Heterojunctions. *ACS Appl. Mater. Inter*. **2012**, *4*, 244-250.
15. Ruderer, M., Hinterstocker, M., Muller-Buschbaum, P. Structure in Ternary Blend Systems for Organic Photovoltaics. *Synthetic Met*. **2011**, *161*, 2001-2005.
16. Chu, C., Tsang, S., Zhou, J., et al. High-Efficiency Inverted Solar Cells Based on a Low Bandgap Polymer with Excellent Air Stability. *Sol. Energ. Mater. and Sol. C* **2012**, *96*, 155–159.
17. Goetzberger, A., Hebling, C., Chock, H. Photovoltaic Materials, History, Status and Outlook. *Mater. Sci. Eng. R* **2003**, *40*, 1.
18. Habas, S., Platt, H., van Hest, M., et al. Low-Cost Inorganic Solar Cells: From Ink to Printed Device. *Chem. Rev*. **2010**, *110*, 6571-6594.

19. Goetzberger, A., Hebling, C. Photovoltaic Materials, Past, Present, and Future. *Sol. Energ. Mater. and Sol. C* **2000**, *62*, 1-19.
20. Yu, G., Gao, J., Hummelen, J.C., et al. Polymer Photovoltaic Cells: Enhanced Efficiencies via a Network of Internal Donor-Acceptor Heterojunctions. *Science* **1995**, *270*, 1789-1791.
21. Chapin, D., Fuller, C., Pearson, G. A New Silicon P-N Junction Photocell for Converting Solar Radiation into Electric Power. *J. Appl. Phys.* **1954**, *25*, 676.
22. Krebs, F. Jorgensen, M., Norrman, K., et al. A Complete Process for Production of Flexible Large Area Polymer Solar Cells Entirely Using Screen Printing - First Public Demonstration. *Sol. Energ. Mater. and Sol. C* **2009**, *93*, 422–441.
23. Wang, Y., Wei, W., Liu, X., et al. Research Progress on Polymer Heterojunction Solar Cells. *Sol. Energ. Mater. and Sol. C* **2012**, *98*, 129–145.
24. Benanti, T., Venkataraman, D. Organic Solar Cells: An Overview Focusing on Active Layer Morphology. *Photosynth Rev*. **2006**, *87*, 73-81.
25. Yang, L., Xu, H., Tian, H., et al. Effect of Cathode Buffer Layer on the Stability of Polymer Bulk Heterojunction Solar Cells. *Sol. Energ. Mater. and Sol. C* **2010**, *94*, 1831-1834.
26. Jun, G., Jin, S., Park, S., Jeon, S., Hong, S. Highly Dispersed Carbon Nanotubes in Organic Media for Polymer Fullerene Photovoltaic Devices. *Carbon* **2012**, *50*, 40-46.
27. Peet, J., Kim, J., Coates, N., et al. Efficiency Enhancement in Low-Bandgap Polymer Solar Cells by Processing with Alkane Dithiols. *Nat. Mater.* **2007**, *6*, 497-500.
28. Kroon, R., Lenes, M., Hummelen, J., et al. Small Bandgap Polymers for Organic Solar Cells (Polymer Material Development in the Last 5 Years). *Polym. Rev.* **2008**, *48*, 531–582.
29. Cai, T., Zhou, Y., Wang, E., et al. Low Bandgap Polymers Synthesized by $FeCl_3$ Oxidative Polymerization. *Sol. Energ. Mater. and Sol. C* **2010**, *94*, 1275–1281.
30. Chen, C. Low-Bandgap Poly(thiophene-phenylene-thiophene) Derivatives with Broaden Absorption Spectra for Use in High-Performance Bulk-Heterojunction Polymer Solar Cells. *J. Am. Chem. Soc*. **2008**, *130*, 12828-12833.
31. Krebs, F., Gevorgyan, S. A Round Robin Study of Flexible Large-Area Roll-to-Roll Processed Polymer Solar Cell Modules. *Sol. Energ. Mater. and Sol. C* **2009**, *93*, 1968–1977.
32. Wu, J., Chen, F., Hsiao, Y. et al. Surface Plasmonic Effects of Metallic Nanoparticles on the Performance of Polymer Bulk Heterojunction Solar Cells. *ACS Nano* **2011**, *5*, 959-967.
33. Kim, S., Na, S., Jo, J., et al. Plasmon Enhanced Performance of Organic Solar Cells Using Electrodeposited Ag Nanoparticles. *App. Phys. Lett.* **2008**, *93*, 73307-73310.
34. Schvets, G. Photonics: Metamaterials Add an Extra Dimension. *Nat. Mater*. **2008**, *7*, 7-8.
35. Evanoff, D., Chumanov, G. Synthesis and Optical Properties of Silver Nanoparticles and Arrays. *ChemPhysChem* **2005**, *6*, 1221-1231.

36. Rycenga, M., Cobley, C., Zeng, J. Controlling the Synthesis and Assembly of Silver Nanostructures for Plasmonic Applications. *Chem. Rev*. **2011**, *111*, 3669-3712.
37. Evanoff, D., Zimmerman, P., Chumanov, G. Synthesis of Metal-Teflon AF Nanocomposites by Solution-Phase Methods. *Adv. Mater.* **2005**, *17*, 1905-1908.
38. Natsuki, J., Abe, T. Synthesis of Pure Colloidal Silver Nanoparticles with High Electroconductivity for Printed Electronic Circuits - The Effect of Amines on Their Formation in Aqueous Media. *J. Colloid Interf. Sci*. **2011**, *359*, 19-23.
39. Shen, C., Hui, C., Yang, T., et al. Monodisperse Noble-Metal Nanoparticles and Their Surface-Enhanced Raman Scattering Properties. *Chem. Mater*. **2008,** *20*, 6939–6944.
40. Griffo, M., S. Carter, A. Holt. Enhanced Photoluminescence of Conjugated Polymer Thin Films on Nanostructured Silver. *J Lumin*. **2011**, *131*, 1594–1598.
41. Lee, S., H. Chon, S. Yoon, et al. Fabrication of SERS-Fluorescence Dual Modal Nanoprobes and Application to Multiplex Cancer Cell Imaging. *Nanoscale*. **2012**, *4*, 124.
42. Petryayeva, E., Krull, U. Localized Surface Plasmon Resonance Nanostructures, Bioassays and Biosensing - A Review. *Analytica Chimica Act.* **2011**, *706*, 8– 24.
43. Link, S., El-Sayed, M. Size and Temperature Dependence of the Plasmon Absorption of Colloidal Gold Nanoparticles. *J. Phys. Chem. B* **1999**, *103*, 4212-4217.
44. Niesen, B., Rand, B., Van Dorpe, P., et al. Excitation of Multiple Dipole Surface Plasmon Resonances in Spherical Silver Nanoparticles. *Opt. Express*. **2010**, *18*, 19032-19038.
45. Sonnichsen, C., Franzl, T., Wilk, T., et al. Drastic Reduction of Plasmon Damping in Gold Nanorods. *Phys. Rev. Lett*. **2002**, *88*, 7.
46. Qu, D., Liu, F., Huang, Y., et al. Mechanism of Optical Absorption Enhancement in Thin Film Organic Solar Cells with Plasmonic Metal Nanoparticles. *Opt. Express*. **2011**, *19*, 24795-24803.
47. Fort, E., Gresillon, S. Surface Enhanced Fluorescence. *J. Phys. D: App. Phys*. **2008**, *41*, 31.
48. Lakowicz, J., Geddes, C., Gryczynski, I., et al. Advances in Surface-Enhanced Fluorescence. *J. Fluoresc*. **2004**, *14*, 425-441.
49. Weitz, Garoff, S., Hanson, C., et al. Fluorescent Lifetimes of Molecules on Silver-Island Films. *Opt. Lett*. **1982**, *7*, 89-91.
50. Sanchez-Gonzalez, A., Corni, S., Mennucci, B. Surface-Enhanced Fluorescence within a Metal Nanoparticle Array - The Role of Solvent and Plasmon Couplings. *J. Phys. Chem. C* **2011**, *115*, 5450-5460.
51. Chumanov, G., Sokolov, K., Gregory, B., et al. Colloidal Metal Films as a Substrate for Surface-Enhanced Spectroscopy. *J. Phys. Chem*. **1995**, *99*, 9466-9471.
52. Zheng, H., Xu, L., Zhang, Z. et al. Fluorescence Enhancement of Acridine Organe in a Water Solution by Au Nanoparticles. *Sci. China Phys. Mech*. **2010**, *53*, 1799-1804.

53. Zhu, J. Zhu, K., Huang, L. Using Gold Colloid Nanoparticles to Modulate the Surface-Enhanced Fluorescence of Rhodamine B. *Phys. Lett. A* **2008**, *372*, 8283-3288.
54. Iosin, M., Baldeck, P., Astilean, S. Plasmon-Enhanced Fluorescence of Dye Molecules. *Nucl. Instrum. Meth. B* **2009**, *267*, 403-405.
55. Heo, M., Cho, H., Jung, J. et al. High-Performance Organic Optoelectronic Devices Enhanced by Surface Plasmon Resonance. *Adv. Mater*. **2011**, *23*, 5689-5693.
56. Wang, Y., Li, Z., Li, H., et al. A Novel Aptasensor Based on Silver Nanoparticle-Enhanced Fluorescence. *Biosens. Bioelectron*. **2012**, *32*, 76– 81.
57. Li, J., Huang, Y., Ding, Y. Shell-Isolated Nanoparticle-Enhanced Raman Spectroscopy. *Nature* **2010**, *464*, 392-395.
58. Lin, S., Wong, M., Pat, P., et al. Cadmium Sulfide Silver Nanoplate Hybrid Structure Synthesis and Fluorescence Enhancement. *J. Phys. Chem. C* **2011**, *115*, 21604-21609.
59. Guerrero, A., Aroca, R. Surface-Enhanced Fluorescence with Shell-Isolated Nanoparticles (SHINEF). *Angew. Chem. Int. Edit*. **2011**, *50*, 665-668.
60. Luu, Q., Doorn, J., Berry, M. Preparation and Optical Properties of Silver Nanowires and Silver-Nanowire Thin Films. *J. Colloid. Interf. Sci*. **2011**, *356*, 151-158.
61. Wang, Q., Lin, S., Ming, C., et al. Plasmon-Enhanced Luminescence of Eu Complex by Using Silver Nanocubes for Different Excitations. *Mater. Lett*. **2011**, *65*, 905-907.
62. Yakasuni, R., Laurent, G., Okazaki, K., et al. Modification of Excimer Emission of Perylene Dye Thin Films by Single Silver Nanocubes. *J. Photoch. Photobio. A* **2011**, *221*, 194-198.
63. Zhao, X.; Zhan, X. Electronic Transporting Semi-Conducting Polymers in Organic Electronics. *Chem. Soc. Rev*. **2011**, *40*, 3728-3743.
64. Koch, N. Organic Electronic Devices and Their Functional Interfaces. *ChemPhysChem* **2007**, *8*, 1438-1455.
65. Evanoff, D. D.; Chumanov, G. Size-Controlled Synthesis of Nanoparticles. 1. "Silver Only" Aqueous Suspensions Via Hydrogen Reduction. *J. Phys. Chem. B* **2004**, *108*, 13948-13956.
66. Evanoff, D. D.; Chumanov, G. Size-Controlled Synthesis of Nanoparticles. 2. Measurement of Extinction, Scattering, and Absorption Cross-Sections. *J. Phys. Chem. B* **2004**, *108*, 13957-13962.
67. Malynych, S., Luzinov, I., Chumanov, G. Poly(Vinyl Pyridine) as a Universal Surface Modifier for Immoblization of Nanoparticles. *J. Phys. Chem. B* **2002**, *106*, 1280-1285.
68. Banerji, N., Cowan, S., Vauthey, E., et al. Ultrafast Relaxation of the Poly(3-hexylthiophene) Emission Spectrum. *J. Phys. Chem. C* **2011**, *115*, 9726-9739.
69. Hu, Z., Tenery, D., Bonner, M., et al. Correlation Between Spectroscopic and Morphological Properties of Composite P3HT/PCBM Nanoparticles Studied by Single Particle Spectroscopy. *J. Lumin*. **2010**, *130*, 771-780.

70. Wang, Y., Kurunthu, D., Scott, G., et al. Fluorescence Quenching in Conjugated Polymers Blended with Reduced Graphitic Oxide. *J. Phys. Chem. C* **2010**, *114*, 4153-4159.
71. Mauer, R., Kastler, M., Laquai, F. The Impact of Polymer Regioregularity on Charge Transport and Efficiency on P3HT:PCBM Photovoltaic Devices. *Adv. Funct. Mater.* **2010**, *20*, 2085-2092.
72. Malynych, S., Chumanov, G. Light-Induced Coherent Interactions Between Silver Nanoparticles in Two-Dimensional Arrays. *J. Am. Chem. Soc.* **2003**, *125*, 2896-2898.
73. Maylynch, S., Chumanov, G. Narrow Plasmon Mode in 2D Arrays of Silver Nanoparticles Self-Assembled on Thin Silver Films. *J. Microsc.* **2008**, *229*, 567-574.
74. Yang, T., Su, T., Lin, P., et al. Fabrication of Porous Polylactic Acid Films Assisted by Dip-Coating and Template Leaching Techniques. *J. Appl. Polym. Sci.* **2012**, *124*, 2333-2339.
75. Perfetti, G., Alphazan, T., van Hee, P., et al. Relation Between Surface Roughness of Free Films and Process Parameters in Spray Coating. *Eur. J. Pharm. Sci*. **2011**, *42*, 262-272.
76. Zeng, X., Kong, X., Ge, J., et al. Effect Solution Mixing Method to Fabricate Highly Transparent and Optical Functional Organic-Inorganic Nanocomposite Film. *Ind. Eng. Chem. Res*. **2011**, *50*, 3253-3258.